UNIVERSITY OF CRETE

MATERIAL SCIENCE DEPARTMENT

PHOTOELECTROCHEMICAL ETCHING FOR FABRICATION OF GAN BASED AIRGAP DBRs MEMBRANES

CHARKOUTSAKI ILIANNA

THESIS COMMETE

Paulos Savvidis, George Deligeorgis, Nicolaos Pelekanos

22/5/2020

Ευχαριστίες

Θα ήθελα να ευχαριστήσω τον επιβλέπων καθηγητή μου Κύριο Παύλο Σαββίδη, που μου έδωσε την ευκαιρία να εργαστώ πάνω στο συγκεκριμένο αντικείμενο, για την επιστημονική υποστήριξη και τις γνώσεις που μου προσέφερε αυτό το διάστημα καθώς και όλη την εργαστηριακή του ομάδα.

Ακόμα, θα ήθελα να ευχαριστήσω τον Πατέρα μου που με την υποστήριξή του όλα αυτά τα χρόνια κατέστησε εφικτή την πραγματοποίηση των στόχων μου.

ABSTRACT

The last decades there is an intense interest on Galium Nitride (GaN) as a semiconductor material of direct energy gap, which belongs to III semiconductor groups, due to the enhanced optical properties that it can offer.

The most recent use of this material lies to the fabrication of Distributed Bragg Reflectors, which are periodic structures formed from alternating layers of materials. These semiconductor layers present an optical path length that equals $\lambda = \lambda_0/4$, where λ_0 is the Bragg wavelength and their reflectivity is influenced by the number of periods and the different refractive indexes. The main asset of these hetero-structures is that within a range of frequencies and with minimum amount of loses, they are able to attain almost total reflection.

Due to the elevated performance that they demonstrate, devices such as vertical-cavity surface emitting layers (VCSELs) can be benefited. However, several challenges have arisen caused by the restriction on the index contrast that these alloys structures provide. To overcome these challenges for the approach of a high reflectivity value, a considerable number of periods must be used, however, despite the lattice match, the constraintment on the index contrast remains a challenge.

In this thesis, theoretical DBRs models were created and by taking advantage of the electrochemical properties and the selective nature of Photo-electrochemical Etching (PEC) process, we proceed to the fabrication of Air-Gap, GaN based DBRs with four alternating periods of GaN and Air, for the obtainment of a wider contrast in refractive index to achieve higher reflectivity. PEC etching is a process that involves electrochemical reactions of semiconductors caused by photo-stimulation when they come in contact with electrolytes (in our case KOH solution). This process presents useful properties such as light-intensity dependence or band gap selectivity and is characterized by minimal “damage” on the surface of the material, in room temperature conditions, and faster etching speed compared to the dry plasma etching technique, which can cause large unevenness to the sidewalls of the membranes.

Finally, considering the state of the art of this procedure and by taking advantage the fundamental principles of modern optics, a set up capable of conducting micro-photo-electrochemical etching, for better experimental results, was created.

Contents

Figures

CHAPTER 1: SEMICONDUCTORS

1.1 Introduction

In periodic structures, the propagation of electromagnetic waves has contributed to many useful technological applications in optoelectronic devices. One material that offers many advantages concerning these devices is Gallium Nitride (GaN), which is a hetero-structure that provides high power and frequency devices. [1][2]

In the late 1960s, the GaN structure was developed on sapphire substrates with the chemical vapor deposition (MOCVD) method from H.P. Maruska and J.J. Teitjen. It is a semiconductor material that belongs to the category of type III-V semiconductors and presents very important properties such as high thermal conductivity and light emission from infrared to ultraviolet. [3]

During the 1980s, Hagen and Baranov demonstrated that Nitride-III and their alloys, such as AlGaN, could be synthesized on a large scale. This specific category of materials is of great scientific interest because they are semiconductor systems in which the defects that they present during fabrication do not seriously affect their optical properties. [3]

From the early 90s, GaN based devices such as laser diodes and blue light emitting diodes (LDs and LEDs respectively), have reformed the technologies in this scientific field, and at the end of that decade, reports of an optically- pumped InGaN based VSCEL device took place. In about 2008, electrically injected InGaN VCSELs were validated, but despite the fact that the experimental focus is on the pursuit of GaN based VCSELs, they have not been commercialized. It has been understood that the key factor behind the success of these types of devices is the DBRs. In the last decades, studies show that the best way for the fabrication of these periodic hetero-structures, is the Photo-electrochemical etching. [1]

Electrochemistry in semiconductors is the basis for understanding the fundamental mechanisms of etching, which are deposition and corrosion. The PEC – etching experimental method was originally developed by Minsky to engrave Group –III Nitride materials at room temperature due to the need for optical components and systems of a specific light wavelength. This is a process that involves electrochemical reactions between a semiconductor and liquid when they are light-stimulated and it is an essential tool for the processing and fabrication of enhanced based nitride-III/GaN optoelectronic devices. [3] [4]

The minority carriers, caused by light in the structure, can simulate the reactions of etching and deposition. Compared to other etching techniques, it is the only promising method available and capable of achieving selective lateral etching and also preserving the optical properties of the based GaN structures, something that will be useful for the fabrication of the DBRs. [4]

In the past years, most of the processing of nitride III structures was carried out by dry plasma etching due to the strong chemical stability of Ga-polar GaN and due to the high resistance that presents to all kinds of solutions at room temperature. This behavior is attributed to the fact that group III nitrides have high bonding energies compared to conventional III-V semiconductors. [5]

The construction of this thesis covers the basic physics of semiconductors, which includes the charge transfer reactions and the non-equilibrium states, in **Chapter 1**. Afterwards, in **Chapter 2**,

the main idea behind the DBRs will be analyzed, along with the theoretical models that were created for ideal reflectivity results, the samples that were used and their characterization processes. Furthermore, in **Chapter 3,** the electrochemistry behind the PEC wet selective etching will be analyzed, for the extraction of GaN based DBRs from GaN/InGaN hetero-structures, were the InGaN has the role of the sacrificial layer. In addition, through the experimental measurements, the appropriate parameters that are related with the reverse bias, the concentration of the electrolyte and the light intensity will be taken. The acquisition of smooth membranes taken by the experimental process, catalyzes their subsequent use to create micro-cavities. Through a specific sample given for the study, the experiment yielded membranes with air-gaps. This can lead to an increase in the refractive index of the cavity that can be created and therefore enhanced optical properties. In addition, by taking advantage of the experimental results, there has been an effort to transfer the procedure to a microscopic level for better data. Finally, in **Chapter 4**, the road that must be followed for the creation of the ideal micro-cavity based on the data that were taken will be discussed.

1.2 Basic Physics

For electrons that move freely in space, there are two important laws that are used to describe their properties. The law of conservation of momentum and the Newton's second law of motion. According to quantum mechanics and classical relations, an electron that moves freely in space can be described by the following equation: [6] [7]

$$\lambda = \frac{h}{\rho} \tag{1.1}$$

where ρ, is the product of the electron mass (m), and the electron velocity (v), λ is the wavelength, and *h* is the Planck constant. The electron wave can also be described through the wave vector k as: [6] [7]

$$\lambda = \frac{2\pi}{k} \tag{1.2}$$

From the combination of these two equations, it is shown that the wave vector is proportional to the momentum and can be defined as:

$$k = \frac{2\pi}{h}\rho \tag{1.3}$$

The kinetic energy of a free electron is given by:

$$\mathrm{E} = \frac{h^2}{8m\pi^2}k^2 \tag{1.4}$$

The relation between the kinetic energy and the wave vector is parabolic, as can be seen from the above eq. (1.4), and is illustrated in **Fig. 1.1**. [6] [7]

In the majority of crystalline solids such as metals, the band structure can be derived by resolving the Schrödinger equation from the perspective of one electron situation. In a semiconductor's case, where the electrons do not move freely, the problem can be approached by Bloch theory where the Schrödinger equation can be written as: [6] [7] [8]

$$[-\frac{h^2}{2\pi^2}\nabla^2 + V(r)]\Psi_k(r) = E_k\Psi_k(r) \quad (1.5)$$

Where V is the potential energy, r the position eigenvector and Ψ(r) the wave equation.

The relation between E and k presents the semiconductor's band structure, which is easier to be determined within the first Brillouin zone. The Brillouin zone can be described as a volume where the values of k vary from k = 0 to some finite values with $k_{max} = \pi/\alpha$. [6] [7] [9]

The band structure is presented as two energy bands, the conduction CB and the valence VB band, separated by an energy gap Eg. For the majority of semiconductors, the top of the valence band is at k = 0. If in an energy diagram the top of the valence band and the bottom of the conduction band are presented for the same value of wave vector k = 0, then the semiconductor is considered to have a direct energy band gap. In indirect energy gap semiconductors, the values of the top of the valence and the bottom of the conduction band do not coincide with the k vector. [9]

In **Fig.1.1 b** and **c**, the band diagrams are illustrated.

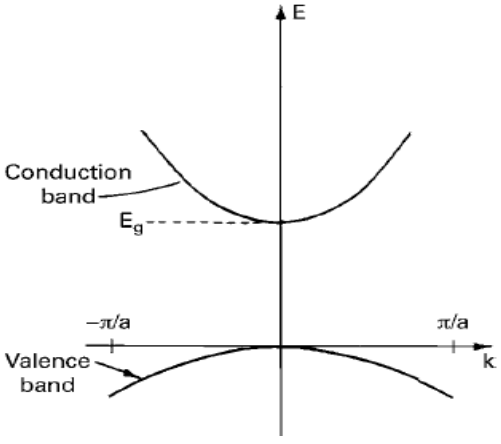

(a)

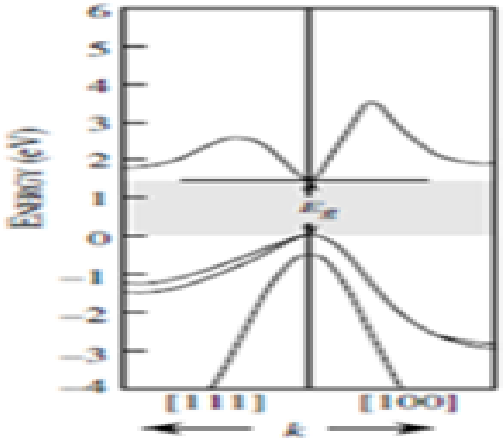

(b)

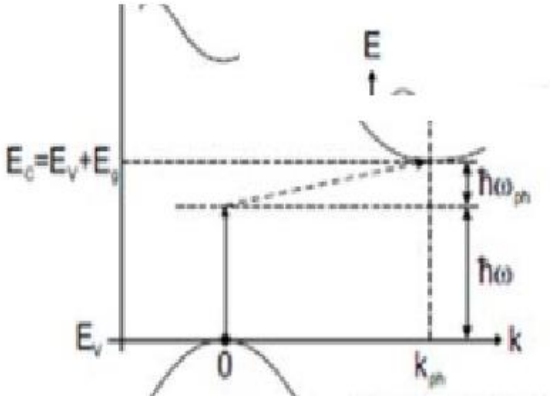

***Figure 1.1**: Electron energy vs k in a semiconductor, b) direct energy band gap of a semiconductor and c) representation of indirect energy band gap. [4]*

For the usage of the free electron approach, the kinetic energy will be defined by the effective electron mass, m^*, that equals to:

$$m^* = \frac{h^2}{4\pi^2}\frac{1}{(d^2E/d^2k)} \tag{1.6}$$

From this relation it is clear that the second derivative of the E – k curve determines the effective mass. In addition, it is understood that the width of the energy band is affected. If the m* gives a small value then the energy bandwidth is wider, otherwise, for large values, the width grows smaller.

Furthermore, from the effective mass equation it is determined that the negative curvature presented for the VB results to negative electron mass. Because this negative electron mass is not obtainable, the occupied orbitals in this band are attributed to holes, which are particles with positive charge. [4][6][7][9]

In addition, it is important to note that E (k) is a function of a 3D wave vector within the Brillouin zone that depends on the crystal structure of the material, and is in agreement with the unit cell of the reciprocal lattice.

1.3 Crystal Structures

To understand the definition of a crystal structure one must realize that a lattice (grid) represents a set of points in space that form a periodic structure. An important property of the lattice is the ability to define three vectors a_1, a_2, a_3, so that any lattice point R' can be extracted by any other point R, so that:

$$R' = R + m_1a_1 + m_2a_2 + m_3a_3 \tag{1.7}$$

where m_1, m_2, m_3 are integers. [7] [8]

The various types of crystal structures that exist can be described by their symmetry groups. The majority of semiconductors that are of direct interest, such as GaAs or AlAs, present a Zinc Blende structure that is formed by groups of unit cubic cells, thus, presenting a higher degree of crystalline symmetry because its lattice constants are equal to the three vertical directions. However, there are various heterostructures of semiconductors, such as GaN, InN or AlN, that present the Wurtzite structure, which is hexagonal and has a hcp cell with two lattice constants (α and γ). In **Fig 1.2 (a)**, these two structures are shown. [7][8]

In Room temperature conditions, the Wurtzite structure is thermodynamically more stable and for that reason the majority of Nitride – III groups tend to crystallize in this phase. The three parameters that define this hexagonal lattice are the length of the hexagon base (a), the height of the hexagonal prism (c) and the ratio of the length of the cation-anion bond along the direction [0001]. In an ideal Wurtzite crystal, the ratio of c/a lattice constant equals to $^{c}/_{a} = \frac{\sqrt{8}}{3}$.

According to the literature, GaN's Wurtzite structure presents a direct energy gap, without excitation for temperatures fluctuating from 0 K to 300 K, with energies of 3.510 eV and 3.437 eV respectively. The symmetry of this particular crystal structure, combined with spin – orbit interaction, leads to the division of the valence band into three non-degenerate sub-zones referred to as A (heavy holes), B (light holes) and C split-off zones, which correspond to the visual transitions of the crystal field and the valence bands, as presented in **Fig. 1.2 (b)**. [6]

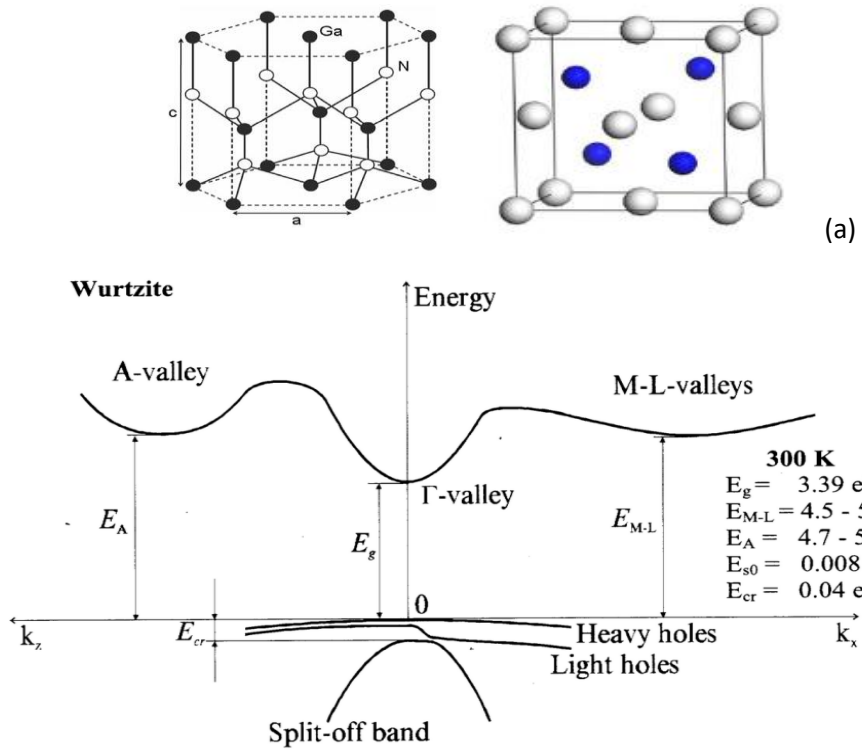

***Figure 1.2**: (a) Crystalline structure of GaN Wrtzite and GaAs Zinc blende respectively, (b) energy diagram of GaN showing the minimum of Cb and the maximum of the Vb. [10][11]*

1.4. Intrinsic and doped semiconductors

Intrinsic are the semiconductors for which the concentration of the electrons n_i equals to the concentration of holes' p_i. The number of electrons is translated as the integral of the Fermi-Dirac distribution function, *f (E),* and the density of energy states and can be written as: [4] [6] [9]

$$n = \int_{E_c}^{\infty} N(E) f(E) dE \tag{1.8}$$

For the hypothesis that $(E-E_F/KT)>>1$, the number of electrons inhabiting the levels of the C_B equals to:

$$n = N_c \exp\left(\frac{E_F - E_c}{KT}\right) \tag{1.9}$$

where N_c refers to the density of energy states within a few KT exciding the C_B edge and E_F is the fermi energy. Following the same conjectures, the hole density near the top of the V_b can be obtained by the equation:

$$p = \int_{-\infty}^{E_v} N(E)\left(1 - f(E)\right) dE \tag{1.10}$$

For the same approximation of the Fermi-Dirac function, the hole density is written as:

$$p = N_v \exp\left(\frac{E_v - E_F}{KT}\right) \tag{1.11}$$

From the above relations, it is derived that the intrinsic electron density *n* can be calculated as:

$$n = n_i p_i \tag{1.12}$$

This equation is also important for a doped semiconductor, because if one concentration is known then the other can also be found. [4] [6] [9]

1.4.1 Doped Semiconductors

Depending on the type of the semiconductor's doping, it can be considered that if conductivity depends on an electron donor, then one can refer to an n-type of semiconductor, otherwise, if it is depended on the acceptor donor- holes, then, the semiconductor is considered as a p-type. [11] [12]

With the addition of impurities in the semiconductor (e.g. acceptor or donors) and by enriching the doping, the semiconductor's Fermi level position moves to the edges of the valence or conduction band. With that presence of impurities of different concentrations in the semiconductor, that are not in an equilibrium state, the equation of *n* equals the sum of the density of ionized donor and the number of holes ($n = N_D^* + p$). The former is connected through the Fermi-Dirac equation to the density of occupied donors (for an n-type semiconductor) through the relation: [4] [6] [12]

$$N_D^* = (1-f)N_D = N_D\left(1-\frac{1}{1+e^{(E_D-E_F)/KT}}\right) \quad (1.13)$$

From the above eq. (1.13), it is concluded that all the donors beneath the Fermi level are ionized. In addition, because the donor concentration is analogous to the density, with the enlargement of the first, the electron density also rises. When this happens, the fermi energy is located between EC and ED. The degeneration of the semiconductor occurs when the concentration of electrons or holes is very high, meaning that all the above relations cannot be applied and the semiconductor demonstrates a more metal-like behavior. All the above approximations can also be applied for the p-type semiconductor. [4] [12]

1.4.2 Excitation and recombination of charge transfer in a semiconductor

As it will be discussed more analytically in ***Chapter 3***, with the application of an external stimulus, such as the excitation of electrons from V_B to C_B, the system of a semiconductor is disrupted but the equilibrium state is more preferable. For that purpose, multiple recombination processes occur, such as the Auger process, which is basically the energy conservation (transfer) to an electron or a hole, or a direct electron-hole recombination. The recombination rate equals to the product of electron and hole concentration with a constant number: [4] [12]

$$R_{pn} = C_o np \quad (1.14)$$

At the time of the excitation process, the concentration of carriers expands by Δn and Δp, respectively.

For an n-type and light intensities, which corresponds to $\Delta n << n$, the recombination rate is given by the relation $R_{pn} = \Delta p C_0 n_0$. From this statement, it is understood that the band-band recombination lifetime and rate lean strongly on the carrier density. The lifetime is given by the following equation: [4] [12]

$$\tau = \frac{1}{(n_o C_o)} \quad (1.15)$$

In the case of a semiconductor such as AlSb that present indirect band gap, what happens is that the process of reconnecting an electron with the hole takes place after the electron is trapped, so it is a two-stage recombination process. From theory, it is known that this convection of the two-stage reconnection offers a wider probability of the electron-hole recombination than the direct vector. The trapping rate equals to: [4] [12]

$$R_c = C_N\left(1-f(t)\right)nN_t \quad (1.16)$$

where f (t) is the section that the trapped electrons are attended and N_t is the trap density. The fraction of traps at equilibrium state can be described as:

$$f_t^o = \frac{1}{1+e^{(E_t-E_F)/KT}} \quad (1.17)$$

Furthermore, for the fermi energy level equals to trap energy level ($E_F = E_t$), the carrier density is given by:

$$n_1 = N_c e^{(E_t - E_F)/KT} \tag{1.18}$$

and thus, the overall flow of carriers for an n-type semiconductor is given by the following equation:

$$R_n = \gamma_n u_{th} N_t \left[\left(1 - f(t)\right) n - f(t) n_1 \right] \tag{1.19}$$

Where u_{th} demonstrates the carrier thermal velocity and γ_n denotes the electron capture cross-section. These approximations can also be adapted for a p-type semiconductor. [4]

As it will be analyzed further in ***Chapter 3,*** the charge transfer reactions play a catalytically important role in the Photo-electrochemical wet selective etching experimental process of the GaN/InGaN heterostructure, because the doping of the material can dictate the hole procedure.

1.4.3 Quasi-Fermi levels – Non equilibrium state

From the use of external stimulus, such as current flowing, the steady state equilibrium that describes a semiconductor can be disturbed. If photo stimulation with a photon beam takes place, the photoionization and the generation of electron-hole pairs is triggered. In those kinds of situations, the mass-action law, the thermodynamic equilibrium and the Fermi-Dirac approximation that are discussed above, are pulled off from their reciprocal equilibrium and do not apply. This means that the hole and electron densities can no longer be given by the same Fermi levels. When this happens, the density of the carriers can be described by two quasi-Fermi levels, E_{Fn} for electrons and E_{Fp} for holes. The following relations elucidate the quasi-Fermi levels, which are: [4]

$$E_{Fn} = E_c - \ln\left(\frac{N_c}{n}\right) \tag{1.20}$$

and for holes:

$$E_{Fp} = E_v + \ln\left(\frac{N_v}{p}\right) \tag{1.21}$$

For a doped n-type material under photo-stimulation where the assumption of $\Delta n << n_0$ is considered, one can observe that the quasi-fermi level of the hole is shifted downwards, while for the electrons it remains the same.

In many cases, near the sample surface the excitation of electron – hole pairs can take place because the infiltration of light is small, resulting in a splitting of the quasi-Fermi levels near the surface and, since the carriers diffuse out of the excitation range and recombine, the quasi-Fermi level of holes varies with distance from the area that is excited. [4]

The electrochemical reactions are motivated by thermodynamic forces, which are relative to the position of the quasi-Fermi levels in respect to the electrolyte. Thus, the quasi-Fermi level have

an important role in electrochemical procedures that take place at the semiconductor/electrolyte interface. In the next **Fig. 1.3**, the quasi-Fermi levels are schematically illustrated. [4] [12]

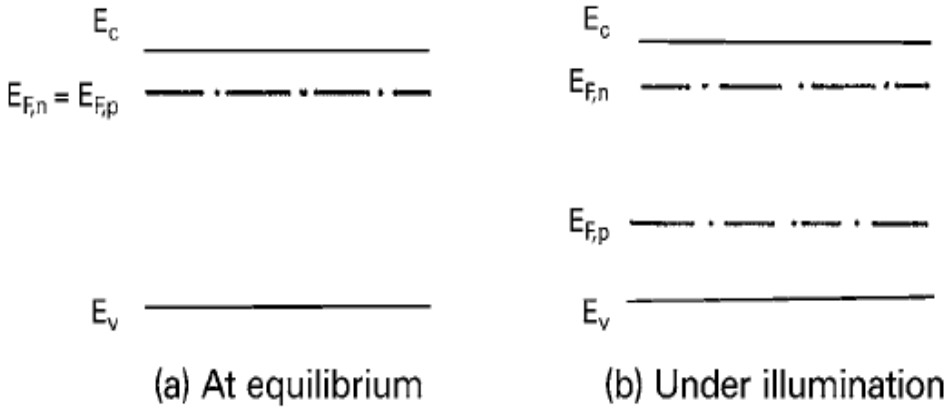

***Figure 1.3**: Quasi-fermi level of carries in semiconductors. [4]*

1.5 Strain and relaxation in crystalline heterostructures

Returning to the crystalline structure, it is important to note that the asymmetry of the lattice can cause mechanical stress, which is due to the elastic behavior of the materials (stress-distortion coupling), which can be described by elastic stiffness. During the fabrication of heterostructures, if a thin film (layer) of material is placed on a substrate, an inter-axial deformation usually appears since the lattice parameters of the layer will be shaped to match the lattice parameters of the substrate, as this leads to a better equilibrium thus, to the least possible deformation of energy. For the deformation of the substrate, a bigger amount of energy would be required and the elastic relaxation would only take place perpendicular to the surface. [6] [14] [15]

To portray the ideal state in the hexagonal lattice, the fundamental lattice constants and the dimensionless internal constant, a_0, c_0, and u_0 respectively, of the Wurtzite crystal structure must be taken into account. From the fundamental constants of the GaN structure, the real stress-deformation vectors can be found. [14]

The disorders that are oriented parallel to the c-axis of the crystal can be considered as single-axon or inter-axial stress, whether it is stress or strain. The deformation factor, ε, is given by: [15]

$$\varepsilon_{xx} = e_{yy} = \frac{(a - a_o)}{a_o} \tag{1.22}$$

$$\varepsilon_{zz} = \frac{(C - C_o)}{C_o} \tag{1.23}$$

From Hooke's law, it is possible to extract the diagonal stress vector of the materials, which is presented by the following equations:

$$\sigma_{\chi\chi} = \sigma_{yy} = \left(C_{1.1} + C_{1.2}\right)\varepsilon_{\chi\chi} + C_{1.3}\varepsilon_{zz} \tag{1.24}$$

$$\sigma_{zz} = 2C_{1.3}\varepsilon_{\chi\chi} + C_{3.3}\varepsilon_{zz} \tag{1.25}$$

For the above equations, the electric field created by spontaneous or piezoelectric polarization has not been taken into account because it is considered negligible. [5]

From the Poisson's law, one can describe the reason for the deformation, and the deformation due to the direction of the stress at the plane. For the Wurtzite (Wz) crystalline structure, with σ_{zz} the strain is given by: [5]

$$\varepsilon_{\chi\chi} = \nu\varepsilon_{zz} \tag{1.26}$$

In the single axial stress, the Poisson ratio is given in the equation below: [5]

$$\nu = \frac{C_{1.3}}{C_{1.1} + C_{1.2}} \tag{1.27}$$

Furthermore, by using the Young's model, it is understood that the stress is the product of the Elasticity modulus and the stain, where the Young's modulus equals to:

$$E = \frac{C_{3.3} - 2C_{1.3}^2}{C_{1.1} + C_{1.2}} \tag{1.28}$$

1.6 References

1. C. Zhang , R. ElAfandy, J. Han, Distributed Bragg Reflectors for GaN-Based Vertical-Cavity Surface-Emitting Lasers, Applied sciences, 2019
2. H. Zhou, M. Diagne, E. Makarona, A. V. Nurmikko, J. Han, K. E. Waldrip, J. J. Figiel, Near ultraviolet optically pumped vertical cavity laser, Electron. Lett. 2000, 36, 1777–1779
3. H.P. Maruska, J.J. Teitjen, Appl. Phys. Lett. 15, 367, 1969
4. R. Memming, Semiconductor Electrochemistry, Second Edition, ISBN: 978-3-527-31281-8
5. M. Trichas, Resonantly Enhanced Selective Photochemical Etching Apl, 2009
6. K. Rajeshwar, Fundamentals of Semiconductor Electrochemistry and Photo electrochemistry, 2007
7. J. Singth, Optoelectronics, ISBN-10: 0070576378, 1995
8. J. M. Wagner, F. Bechstedt, Properties Of Strained Wurtzite Gan And Aln, 2002
9. E. Girginoudi, Semiconductor theory
10. J. Piprek, GaAs 2 Nitride Semiconductor Devices, ISBN-10: 3527406670, 2007
11. I. Vurgaftman, J. R. Meyer, L. R. Ram-Mohan, Band Parameters For III–V Compound semiconductors and their alloys, Journal of Applied Physics 89, 2001

12. L. M. Gleria, Charge transfer processes at large band gap semiconductor electrodes: reactions at SiC-electrodes

13. H. Qin, X. Luan, C. Feng, D. Yang, G. Zhang, Mechanical, Thermodynamic And Electronic Properties Of Wurtzite And Zinc-Blende Gan Crystals, 2001

14. V. N. Brudnyi, A. V. Kosobutsky, N. G. Kolin, Effect of pressure and mechanical stress on the electronic properties of AlN and GaN, Physics of the Solid State volume 53, pages 679–688, 2011

15. W. D. Callister, D. G. Rethwisch, Fundamentals of Materials Science and Engineering, ISBN-10: 1118061608,

CHAPTER 2: TOWARD AIR-GAP DBRs

2.1 Introduction

In this chapter the basic concept of the Distributed Bragg Reflectors (DBRs) and the air-gap DBRs will be analyzed, as well as the advantages that they offer and the challenges that have to be overcomed. Furthermore, through the matrix transfer method, theoretical models of different Distributed Bragg Reflectors and air gap Distributed Bragg Reflectors will be presented, as well as the difference regarding their reflectivity spectrums. Finally, the structures and the mesas patterns, which were later characterized with XRD and Photoluminescence measurements, will also be discussed.

2.2 Distributed Bragg Reflectors and Air – Gap based Nitride III DBRs

Two mirrors facing each other form an optical cavity. The distance between the mirrors, or the width of the cavity, is tuned to accommodate a standing wave of a specific wavelength. When an active medium is tuned to the same energy and is placed inside the cavity, then the whole structure is called a micro-cavity. This structure can trap light of a specific wavelength and force the strong interactions between photons and excitons for the creation of quasiparticles that are called exciton-polaritons. Polaritons are a unique combination of photons and the excitons of a semiconductor, that present different properties from either the matter or the light that combines them.

High reflectivity mirrors are needed in order to insure strong light-matter interaction. DBR mirrors are good candidates because they present higher reflectivity, opposed to the metallic mirror, and because they are semiconductor devices the fabrication of the whole structure with MBE growth is more convenient. Distributed Bragg Reflectors are used in optoelectronics devices to create laser cavities for better optical performance and they consist of pairs of alternating semiconductor materials with individual refractive indexes. The optical path of the semiconductor layer is $\lambda_0/4$, where λ_0 is the Bragg wavelength. The reflectivity of these structures depends on the number of periods and the difference in refractive indexes. [1]

As mentioned, one of the most important advantage of the DBRs is the high reflectivity value. The reflectivity value at λ_0 wavelength is given from the equation:

$$R = 1 - 4\frac{n_{ext}}{n_c}\left(\frac{n_L}{n_H}\right)2N \tag{2.1}$$

Where 2N is the number of layers forming the DBR, n_c the refractive index of the cavity and n_L and n_H the refractive indexes of the low and the high semiconductor layers. As it is observed form the equation above, the reflectivity value grows with a large number of periods and a high range of index contrast. [2]

In the last decades, the experimental work has been focused on the use of DBRs based on nitride - III structures, due to the high performance that they demonstrate in devices such as vertical-cavity surface emitting laser (VCSELs). [3]

However, several challenges have arisen caused by the restriction on the index contrast that these alloys structures provide. To overcome this challenge, a considerable number of periods must be used, as it was reported from *Waldrip et al.* He and his research team described a structure that consisted of a 60-period $Al_{0.2}Ga_{0.8}N$/GaN DBR with a very high reflectivity peak of 99.1% at λ=378nm. [3] [4]

Despite of the lattice match, which is offered from alloys such as $Al_xGa_{1-x}N$/GaN or AlInN/GaN, and the lack of strain relaxation in DBRs structures above the 40 pairs, as mentioned from *Mathieu Bellanger et. al*, the low index contrast remains a challenge. The answer to this problem has been given by developing the technology of fabricating an air gap-based DBR. The air gap-based DBR is structured by repeating alterations of air and III-nitride. In comparison with an epitaxial DBR, the air gap-based one shows a wider stop-band and the alterations of air and nitride-III layers results in a greatly enhanced contrast in refractive index and, thus, increased reflectivity. It is predicted that a peak reflectivity of more than 99% can be achieved by a GaN/air gap-based DBR structure with as few as four periods, as it was reported from R. Sharma et al. [1] [3] [5]

In the next paragraph, an explanation of how the complex physics behind these structures can be normalized will be given and also how to calculate the reflectivity through the scattering and the matrix theory. The reflectivity and wavelength diagrams of theoretical structures of DBRs will also be presented.

2.2.1 Scatter and transmission matrices

When dealing with complex structures such as DBRs, it is easier to use normalized amplitudes. The scattering coefficients can be used for the normalization of the ratio width, when it enters or exits an interface. After that, the scattering matrix can be translated to a transmission matrix. [6]

The definition of a scatter matrix can be given as:

$$\begin{pmatrix} S_{11} & S_{12} \\ S_{21} & S_{22} \end{pmatrix} \begin{pmatrix} a_1 \\ a_2 \end{pmatrix} = \begin{pmatrix} b_1 \\ b_2 \end{pmatrix}$$

For a dielectric interface and if a normal incident plane wave is assumed, then for $\alpha_2 = 0$:

$$S_{11} = \frac{b_1}{a_1} = -r_1 = \frac{n_1 - n_2}{n_1 + n_2} \tag{2.2}$$

Where r_1 is the reflectivity and n_1, n_2 the refractive indexes. If the refractive indexes contrast is considerable, then the reflectivity value grows. In **Fig 2.1** a schematic representation of the interface for two dielectrics exemplifying the planes at interface for both ports is given.

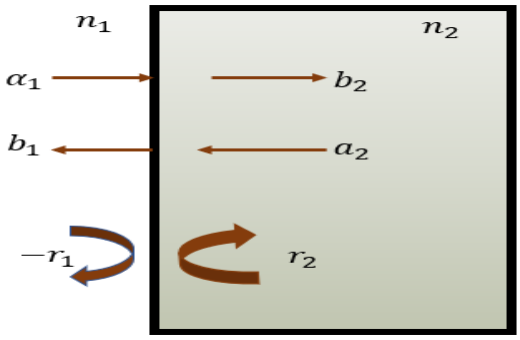

***Figure 2.1**: Schematic Presentation of the interface for two dielectrics exemplifying the planes at interface for both ports.*

Likewise, for α_1=0:

$$S_{22} = \frac{b_2}{a_2} = -(-r_1) = r_2 \tag{2.3}$$

Therefore:

$$S_{12} = S_{21} = \sqrt{1 - r_1^2} \tag{2.4}$$

Eq. 2.4 can be used when a plane wave does not lose power, meaning that it does not travel through a medium with length L, so, there are no losses. For the normally incident plane wave case:

$$S_{12} = S_{21} = \sqrt{1 - r_1^2} = t = \frac{2\sqrt{n_1 n_2}}{n_1 + n_2} \tag{2.5}$$

Thus, the scattering matrix (S) can be described as:

$$S = \begin{pmatrix} -r_1 & t \\ t & r_1 \end{pmatrix} \tag{2.6}$$

The scattering matrix is converted to transmission matrix (T) as:

$$T = \frac{1}{t}\begin{pmatrix} -r_1 & t \\ t & r_1 \end{pmatrix} \tag{2.7}$$

When the ratio of the light travels a distance L inside a medium, then the only thing that changes is a phase shift that equals with: $\phi=\beta_2 L$, where β_2 is a parameter. In this case, (S) is given by: [6] [7]

$$S = \begin{pmatrix} r_{12} & t_{12}e^{-j\varphi} \\ t_{12}e^{-j\varphi} & -r_{12}e^{-2j\varphi} \end{pmatrix} \tag{2.8}$$

Thus:

$$T = \frac{1}{t_{12}} \begin{pmatrix} e^{j\varphi} & r_{12}e^{-j\varphi} \\ r_{12}e^{j\varphi} & e^{-j\varphi} \end{pmatrix} \tag{2.9}$$

The table above refers to one period. For N periods in the structure, the table becomes T^N.

2.2.2 Reflectivity and wavelength diagrams in periodic multilayer structures (DBRs)

As it was mentioned in sub – chapter 2.2, the Distributed Bragg Reflectors are multilayered periodic structures from two different materials with different refractive indexes and they can be used in optoelectronics devices to create laser cavities for better optical performance. The thicknesses of the layers can be defined as d_1 and d_2 and the refractive indexes as n_1 and n_2.

From **Fig. 2.2** presented below, the period of the structure can be calculated.

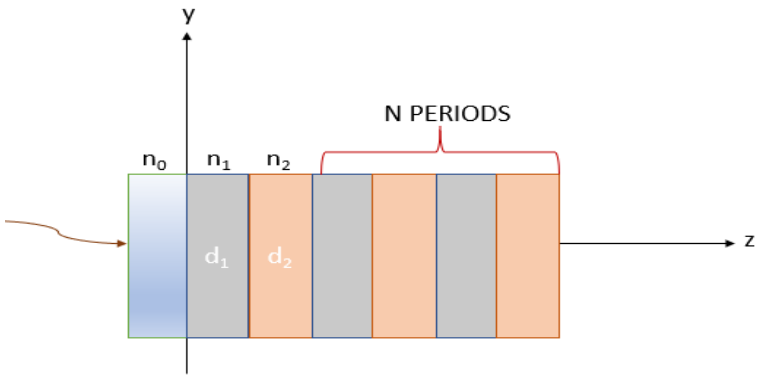

***Figure 2.2**: Representation of a Distributed Bragg Reflector with two different materials.*

The period is given by:

$$Period = \frac{\lambda_o}{4n_1} + \frac{\lambda_o}{4n_2} = d_1 + d_2 \tag{2.10}$$

Consequently, the period can be described as the product of the matrices of an individual layer of the DBR as: [8]

$$Period = M_1 M_2 \tag{2.11}$$

For N number of periods, the matrix of the total structure is written as:

$$M_{tot} = \left(M_1 M_2\right)^N = \left(M_{period}\right)^N \tag{2.12}$$

The reflectivity of these structures equals with: [7]

$$R = \left(\frac{n_0 n_2^{2N} - n_s n_1^{2N}}{n_0 n_2^{2N} + n_s n_1^{2N}} \right)^2 \tag{2.13}$$

For the observation of high reflectivity, a high refractive index contrast is needed. This can be achieved with materials that differ considerably in their lattice constant. In **Fig. 2.3**, the lattice constant and the bandgap energy diagram of Nitride –III based alloys are observed. The problem with these fabrications is that during their growth, one can observe cracks or roughness on the surface of the structure, due to the high lattice mismatch. To overcome this challenge a considerable amount of layers with similar lattice constants must be used for the creation of the DBRs. Airgap DBRS ensure high refractive index contrast with no lattice mismatch**.** In the following **Fig. 2.4** and **2.5**, the relation between the period and the reflectivity through the theoretical models of an AlGaN/GaN DBR, the difference between a GaN/Air-Gap DBR and the calculated reflectivity of the DBRs in their operating wavelength are presented. [9]

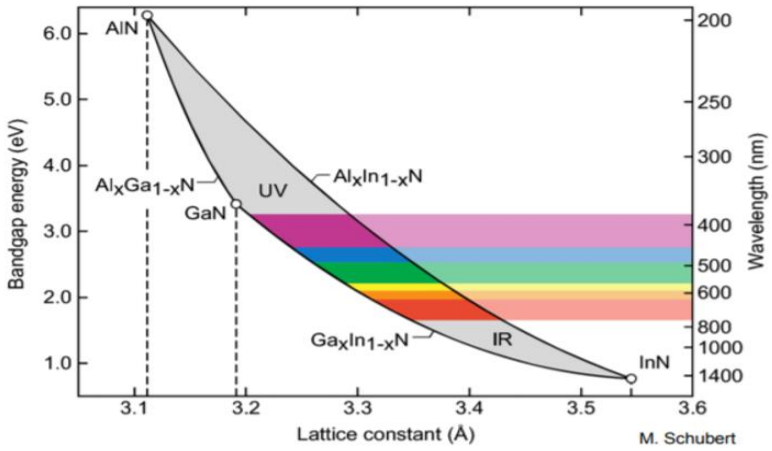

***Figure 2.3**: Lattice constant of Nitride-III based alloys. By M. Schubert.*

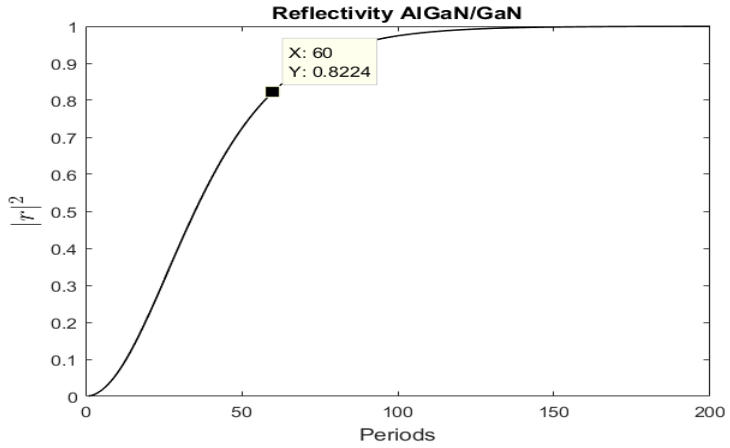

***Figure 2.4**: Relation between Reflectivity and Periods for a theoretical model of $Al_{0.3}GaN_{O.7}$/GaN with refractive indexes n_{AlGaN} = 2.4 and n_{GaN} = 2.3 at λ = 450nm*

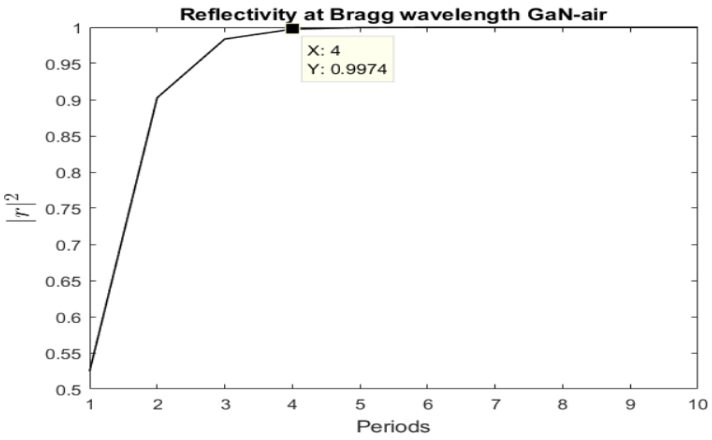

***Figure 2.5**: Relation between reflectivity and periods of GaN/Air-Gap DBR with refractive indexes nGaN =2.5 and nair = 1 at λ = 450nm.*

From the schematic representations above, it is understood that the contrast in the refractive index has a significant role in the value of the reflectivity. Four periods of air-gap offer 99.7% reflectivity, compared with sixty alternating layers of AlGaN/GaN that offer 81%. It also appears, in **Fig. 2.6,** that with one period of GaN-AIRGAP the reflectance value is at about 55%, which is a considerable high value for only one period.

One can also notice the high reflectance bandwidth of these structures. The stop-band width of the DBRs can be defined as $\Delta\lambda_{max,}$ which is given from:

$$\Delta\lambda_{max} = \frac{4\lambda}{\pi}\sin^{-1}\left(\frac{\Delta n}{n_1 + n_2}\right) \tag{2.14}$$

As can be seen, $\Delta\lambda_{max}$ is proportional to the Bragg wavelength and it is related with the refractive index contrast. Furthermore, it describes the full width of the reflectivity at half maximum when the number of the alternating periods comes close to infinity. [9]

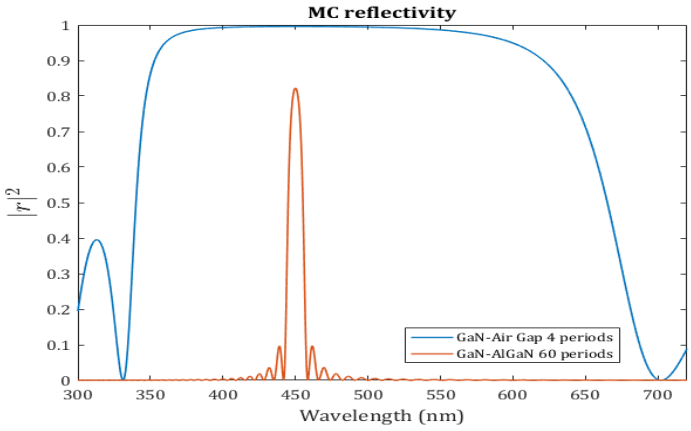

Figure 2.6: Calculated Reflectivity of theoretical DBRs and Air-Gap DBR structures.

The structures of the samples that were used for the creation of the air-gap DBRs through the PEC process (discussed in the next chapter) are due to previous studies that have resulted from a careful design which will contribute to enhanced and improved visual properties in their later use. Their structure will be presented in the next section.

2.3 Sample characterization

Two samples were used for the wet-selective photo-electrochemical etching, which were designed carefully so that the quality of the layer/air-gap pair is the desirable. The first sample (E-3689), consist of a c-GaN/c-Sapphire substrate, the "sacrificial" layer InGaN about 10%, with thickness 25nm and a GaN layer of about 200nm. The fabrication was achieved by the Molecular Beam Epitaxy technique, form the CEA team in Grenoble, France. The second sample (E-3690) consist of a c-Sapphire substrate, a 10 μm thick GaN layer and five alternating layers of GaN and InGaN, where InGaN has again the role of the sacrificial layer for obtaining the air-gap based GaN DBR.

In order to verify the content and the thickness of the different layers of the structures of the samples E-3689 and E-3690 and to determine any derivation from the theoretical values that were given, XRD characterization was performed.

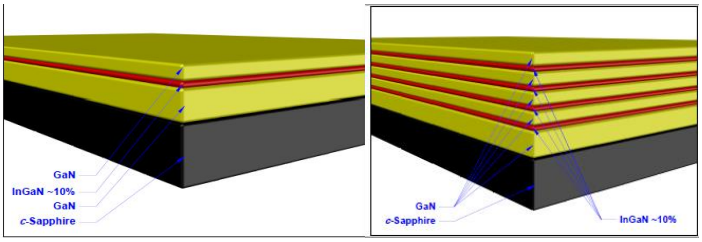

***Figure 2.7**: 3D representation of the samples.*

2.3.1 XR-Diffraction

X-ray diffraction is the reflection of an X-ray by a family of parallel and equally spaced atomic planes. It is a phenomenon where an apparent bend and propagation in a new direction of the waves appears when an X-ray encounters an object. This method enables the qualitative and quantitative analysis of crystalline materials. [10]

When the crystalline material is rotated relative to the X-ray beam at certain angles, the X-rays reflect from the surface of the sample. For these rays, Bragg's law applies. When a monochromatic X-ray beam with a certain wavelength λ hits on the planes of a crystalline lattice at an angle θ, the beam will be diffracted if the path of the reflected rays to the successive planes (with distance d) is an integer multiple of the wavelength. The recording of the diffraction angle and the number of rays at a particular angle θ will give the diffraction spectrum of the materials that are under examination. [10]

The X-ray diffraction (XRD) characterization technique was performed on the samples after their development, in order to determine the thicknesses and the content of the various layers and to examine any deviation from the theoretical values.

In the **Fig. 2.8** and **2.9** below, the ratio of the intensity of the scattered radiation to the angle 2θ (scan angle) is presented.

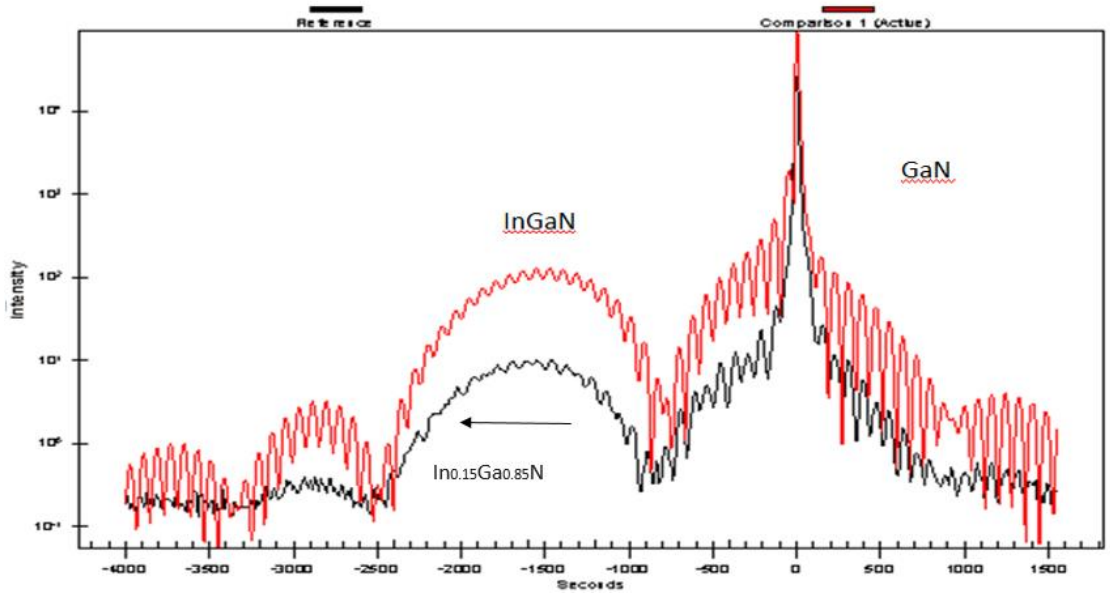

***Figure 2.8**: XRD diagram of sample E-3689 in red, showing the optimally adjusted theoretical curve in relation to the experimental curve (black).*

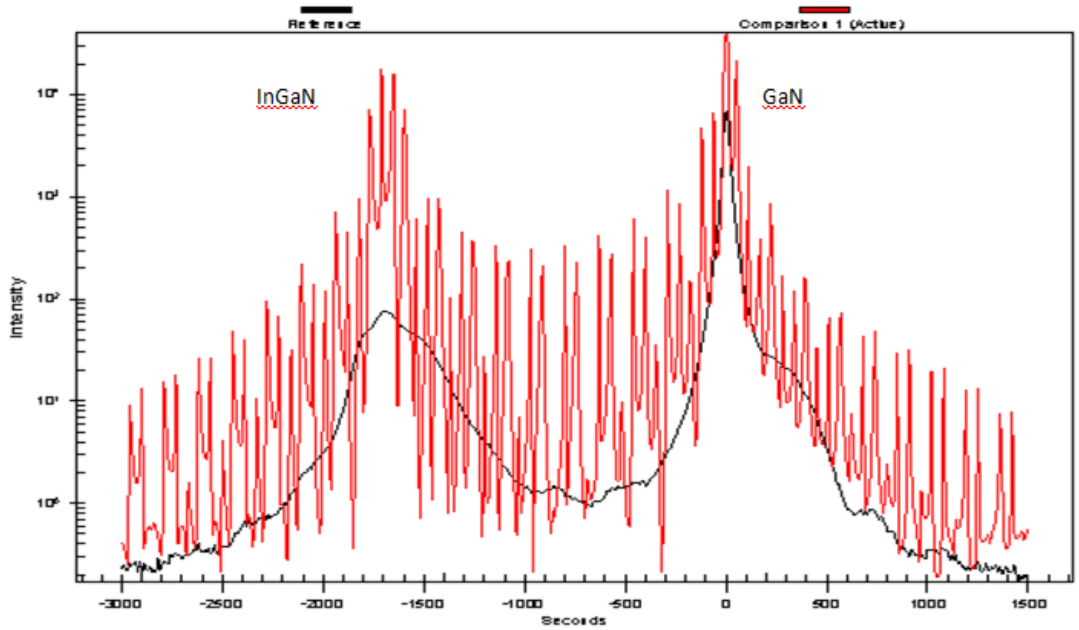

***Figure 2.9**: XRD diagram of sample E-3690 in red, showing the optimally adjusted curve in relation to the experimental measured curve (black)*

Through these measurements, it became known that the thickness of GaN for the E-3689 sample is 195nm while the indium (In) content is 15%. Therefore, the content for the sacrificial layer is $In_{0.15}Ga_{0.85}N$. The results converge quite well with the theoretical values given above. The same measurement was also carried for the sample E-3690, as shown in **Fig 2.9**.

Through **Fig 2.9**, it is observed that the thickness of GaN for E-3690 is 190 nm while the indium content is 15%. Therefore, the content for the alternating sacrificial layers is $In_{0.15}Ga_{0.85}N$. However, this measurement reveals a rather significant deviation from the theoretical values that were given due to the complexity of the structure.

2.3.2 PL Measurements

The term photoluminescence refers to phenomena that are related to energy absorption and subsequent light emission. The PL measurement plays a catalytic role in the characterization of semiconductors and is based on the absorption of monochromatic light having a wider energy gap from the semiconductor, so that the optically generated excitations can recombine and emit light. The spectral region of interest range from ultraviolet radiation to infrared wavelengths. [11]

PL measurements have taken place at room temperature, in order to carry out appropriate information regarding the interface of the semiconductor layers. However, it is more preferable to take measurements at low temperatures in order to avoid thermal excitation of carriers, which extend the bandwidth of a band in the PL spectrum. In addition, it should be borne in mind that when placing the sample in the experimental set up there should be no stress on the sample or the emitted light might change. [11]

For the experimental set up, the laser that was used for the measurements is He-Cd whose radiation is continuous with wavelength λ = 325nm and power at about P = 35mWatt. For samples E-3689, E-3690 photoluminescence measurements (**Fig 2.10**) were carried out at room temperature and performed to provide extra information on the surface and the thicknesses of the samples.

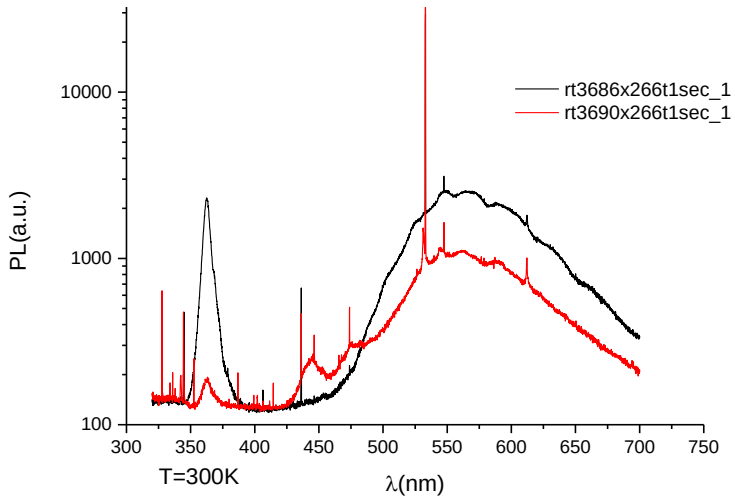

***Figure 2.10**: PL measurement at for E-3689, E-3690 shows the position of the samples at room temperature (300K*

2.4 REFERENCES

1. R. Sharma, Y. S. Choi, C. F. Wang, A. David, C. Weisbuch, S. Nakamura, E. L. Hu, Gallium-nitride-based microcavity light-emitting diodes with air-gap distributed Bragg Reflectors, Applied Physics Letters 91, 2007, 211108.
2. S. Tsitzos, Polarizing Devices of Vertical light Emission.
3. R. Sharma, E. D. Haberer, C. Meier, E. L. Hu, S. Nakamura, Materials Department, University of California, Vertically oriented GaN-based air-gap distributed Bragg reflector structure fabricated using band-gap-selective photo – electrochemical etching, 93106
4. K. E. Waldrip, J. Han, J. J. Figiel, H. Zhou, E. Makarona, A. V.Nurmikko, Stress engineering during metalorganic chemical vapor deposition of AlGaN/GaN distributed Bragg reflectors, Appl. Phys. Lett. 78, 2001, 3205.
5. M. Bellanger, V. Bousquet, G. Christmann, J. Baumberg, M. Kauer, Highly Reflective GaN-Based Air-Gap Distributed Bragg Reflectors Fabricated Using AlInN Wet Etching, Applied physics express 2, 2009, 121003.
6. L. A. Colden, S. W. Corzine, M. L. Masanovic, Diode Lasers and Photonic Integrated Circuits, Second edition, ISBN-10: 9780470484128.
7. Sh. A. Furman, A. V. Tikhonravov, Basics of Optics of Multilayer Systems, Editions Frontieres, 1992.
8. P. Yeh, Optical Waves in Layered Media, Wiley, 2005, ISBN: 978-0-471-73192-4.
9. C. Zhang, R. Elafandy, J. Han, Distributed Bragg Reflectors for GaN-Based Vertical-Cavity Surface-Emitting Lasers, Applied Sciences, 2019.
10. G. Stergioudis, Rays - X (Xrd)
11. C. Ronda, Luminescence From Theory To Applications, New York, 2008

CHAPTER 3. PHOTO-ELECTROCHEMICAL ETCHING

3.1 Introduction

Photo-electrochemical etching is an essential tool for the processing and fabrication of enhanced based nitride-III/GaN optoelectronic devices. Compared to other etching techniques, it is the only promising method available and capable of achieving selective lateral etching, preserving the optical properties of the based GaN structures. [1]

In the past years, most of the processing of nitride III structures was carried out by dry plasma etching due to the strong chemical stability of Ga-polar GaN and due to the high resistance that it presents to all kinds of solutions at room temperature. This behavior is attributed to the fact that the group III nitrides have high bonding energies compared to conventional III-V semiconductors, whose energies are, i.e., (7,7eV/atom) for InN, (8,9Ev/atom) for GaN and (6,5eV/atom) for GaAs. The high bond stability and the wide energy band spectrums make nitrides chemically inert and extremely resistant to bases and acids at room temperature. [1][2]

However, the dry plasma etching technique shows two main disadvantages such as the creation of damage on the structures caused by ions and the difficulty in achieving uniformity at the sidewalls and the surface of the structures, something that is required in many optoelectronic devices such as Ga-based DBRS. On the other hand, the selective photo-electrochemical wet etching (PEC) technology has played an important role in the development and fabrication of these structures. [1]

In this chapter the basic theory of the photo-electrochemical procedure, its properties and the experimental process will be discussed. Furthermore, the experimental set up, the data taken and a new approach of the PEC etching technique, in a microscopic level, will be analyzed.

3.2 Semiconductor – Electrolyte interface at equilibrium

A redox electrolytic solvent exhibits an electrochemical potential, which can be calculated using the Nernst equation and is given:

$$E_{REDOX} = E^{O}_{REDOX} + \frac{RT}{nF}\ln\left(\frac{C_{ox}}{C_{red}}\right) \tag{3.1}$$

where c_{red} refers to the concentration of reduced species and c_{ox} is translated as the concentration of the oxide species. When a semiconductor comes in contact with an electrolyte, the desire match with the semiconductor physics can be accomplished by looking at the oxide elements of an electrolyte as a conduction band and the reduce species as the valence band. [3]

For an n-type semiconductor, the assumption is that the Fermi energy (E_F) is higher than the electrochemical potential of the electrolyte ($E_{F,\ REDOX}$). Thus, there is a charge movement till the two phases come to an equilibrium state, which means that the Fermi level positions in the n-type semiconductor is $E_{F,\ REDOX} = F_{ermi,\ sem/ctor}$, as shown in **Fig 3.1**. During the charge movement from one phase to the other, a band-bending phenomenon is observed at the semiconductor phase.

When this equilibrium state is accomplished, then, a potential is developed which equals with: [2] [3]

$$V_{SC} = -\frac{eN_d W^2}{2\varepsilon_1} \tag{3.2}$$

where W is the depletion layer width, ε_1 is the dielectric constant of the semiconductor and N_d is the concentration of the majority carriers. The region where the charge transfer takes place is called the depletion layer or the space charge region. [2]

When the semiconductor is illuminated with a beam with energy higher than the semiconductor's energy band gap, then, the holes and the electrons in the space charge region are transferred with the help of an electric field and also "diffusion due to the gradient in the carrier concentration". The electric field is given by: [2]

$$\nabla E = \frac{qN_d}{\varepsilon} \tag{3.3}$$

The photo – generated holes react with the solution species at the electrolyte/semiconductor interface, while the energy gap and the electric field act as kinetic barriers for the electrons, preventing them to reach the electrolyte/semiconductor interface. The concentration of holes can be calculated from the equation of the current density (J_h) that equals with: [2] [3]

$$J_h = q\mu_h hE - qD_h \nabla h \tag{3.4}$$

where h represents the concentration of holes, μ_h the mobility of the holes and D refers to the hole diffusion constant.

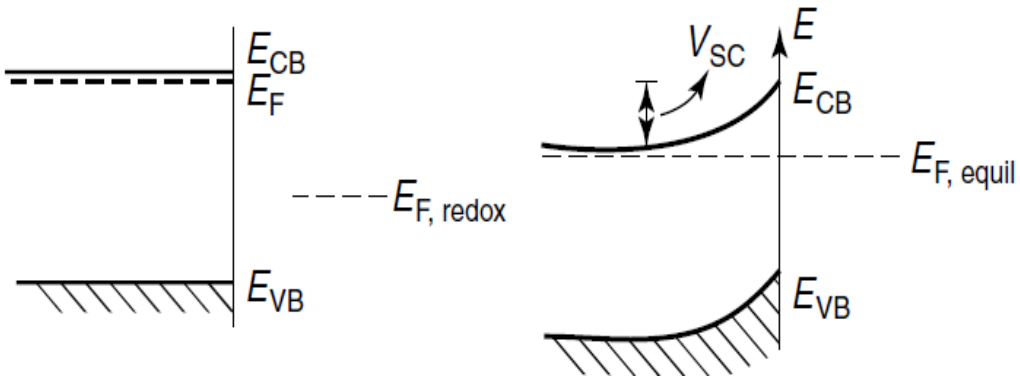

***Figure 3.1**: Semiconductor/electrolyte interface until the equilibrium state EF, REDOX=Fermi, sem/ctor. [3]*

In the experimental PEC etching that took place for the fabrication of the air/GaN based DBRS, the potential of the semiconductor is controlled by a power supply with the application of reverse

bias (V < 0). When applying the reverse bias, an upward bending of the valence and the conduction band is observed. [1]

3.2.1 Charge transfer reactions

When a semiconductor comes in contact with an electrolyte solution and is excited by a beam of light whose energy band-gap is wider than the semiconductor's, then the energy density scattered during the absorption can be described by the following equation: [1]

$$g(x) = I_0 a e^{-ax} \tag{3.5}$$

Where α equals the light absorption coefficient and I_0 characterizes the intensity of light flowing on the semiconductor.

During the illumination of the semiconductor an excess of carriers is created, which results in a change in their concertation (for an n-type semiconductor the minority carriers) and consequently in the quasi-Fermi levels. The charge transfer reaction of these excess carriers that are generated during photo-stimulation leads to the band bending change at the interface and, in addition, they are responsible for the change in the charge distribution that takes place in the depletion layer and hence the electrode potential. The corresponding field creates a potential well that draws the holes to the surface while the electrons are driven to the bulk semiconductor. The next **Fig 3.2** presents the displation of quasi-Fermi level of electrons in relation to the equilibrium Fermi energy level. [3]

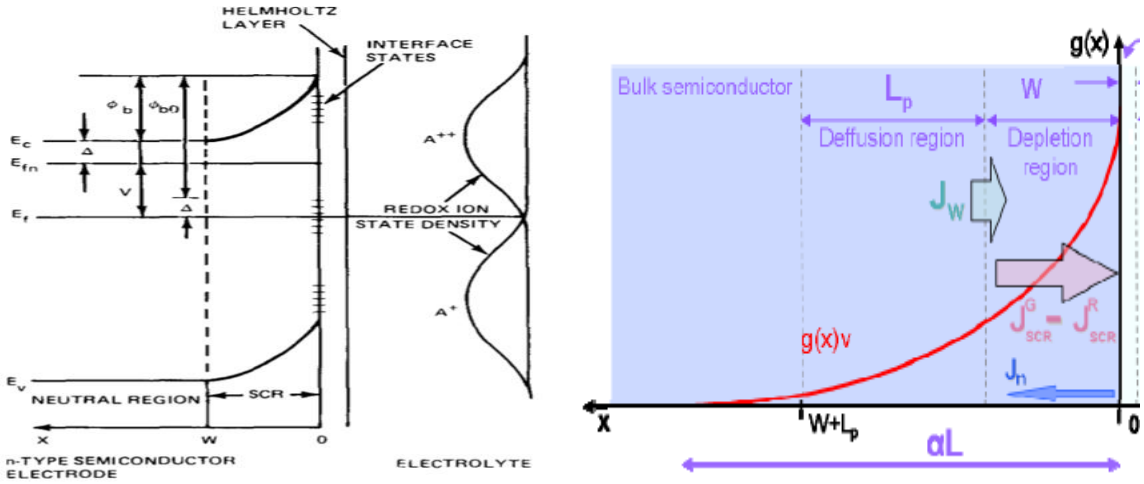

***Figure 3.2**: n-type semiconductor's energy- level diagram under illumination and the function g(x) represented by the red curve. [1][5]*

The current density covering the semiconductor/electrolyte interface, given by the Reichman model, can be described as: [1] [6]

$$J = J_n + \left(J_w + J_{SCR}^G - J_{SCR}^R \right) \tag{3.6}$$

Where the current density created from the photon absorption in the depletion layer (space charge region) and the recombination current density are given, respectively, by the equations: [1][6]

$$J_{SCR}^{G} = qI_o\left(1-e^{-aW}\right) \tag{3.7}$$

$$J_{SCR}^{R} = \frac{n\pi KTWe^{\frac{-qV}{2KT}}}{4\tau\left(V-V_{fB}\right)}\sqrt{\frac{p_s}{p_{so}}} \tag{3.8}$$

where V_{FB} is the flat – Band potential, n the internal carrier density, p_{so} the concentration at the state of equilibrium, p_s the concentration at the excited state. [1] [3]

The current density of holes at the edge of the space charge region is described by the term: [1]

$$J_w = -J_O\left(\frac{P_w}{P_o}-1\right)+\frac{qI_o aL_p e^{-aW}}{1+aL_p} \tag{3.9}$$

where P_0 is the concentration of holes at equilibrium, Pw the hole concentration from the diffusion region and L_p the diffusion region.

For the wider set of n-type semiconductors, the current density of electrons is described by the following equation: [1]

$$J_n = -I_n\left[e^{(-qV/KT)}-1\right] \tag{3.10}$$

From all the above equations, one can conclude that the value of the photocurrent is affected by many factors and parameters. For example, for a doped semiconductor its absorption coefficient and its doping can determine the width of the space charge region, which in its turn also affects the relation $\frac{1}{\alpha} > (W + L_P)$, which determines the recombination region.[2][3][6]

To summarize, the process of Photo – electrochemical etching can be regulated by many factors and parameters related to the intensity of the power of the emitted light, the doped semiconductor itself and the applicable bias, as it will be observed in chapter 3 where the experimental conditions will be explained.

3.2.2 PEC Properties

The Photo-electro-chemical etching processes present useful properties such as light-intensity dependence, or band-gap selectivity that, due to their selective nature, can offer better experimental results, as it will be discussed below. [7]

1. *Band-gap selectivity*: The layers of hetero-structures present different band-gaps thus, the narrower – gap layer can be selectively etched when the material is illuminated with a beam that its spectrum can be absorbed by that specific layer (sacrificial layer), but not by the layer that present a wider band gap in relation to the beam of light. [2] [7]

2. *Dependence of light*: When the light intensity is wider the etch rate grows. A linear correlation between the etch – rate and the light intensity has been observed that takes place due to the photo – generation of the minority – carriers of the semiconductor. [2]
3. *Dopant-type selectivity:* Depending on the type of the semiconductor, that can be either n-type or p-type, one can apply reverse bias to etch n-type materials or forward bias to etch isotropically p-type semiconductors. The p-type semiconductors in a more advanced scheme can be photo-etched without the use of bias. [2]
4. *Band-position selectivity*: Depending on the electrical bias that is applied, the shifts in the valence or the conduction band can be used to selectively etch a specific composition. [2]
5. *Etch-rate and photocurrent monitoring*: It is possible to monitor the sacrificial layer that is removed and the etch rate by measuring the current flow in the external circuit. In addition, it is possible to observe the photocurrent degradation over time, which are inversely proportional. As the time of the etch process increases, a decrease in the photocurrent is observed. [2]
6. *Mechanism and process definition*: The studies of the photo-electrochemical procedures, can offer new results in chemical processes or the optimization of the existing ones. That can happen because one can measure the rate of the individual reactions, which make up complex procedures such as oxidation properties or electro- less processes. [2]

3.3 Experimental setup

The aim of the experimental process is the optimization of the parameters of the PEC etching, as well as, the achievement of extremely smooth surfaces for the GaN-air based distributed Bragg Reflectors, for more advanced optical properties.

The quality of the etching depends on the intensity of a photo-beam that stimulates the InGaN layer and is under the bandgap of the GaN layer, a reverse bias that will be applied through the machine Keithley 6517 and the molarity of the electrolyte.

As discussed in the second chapter, two samples were used for the creation of the one pair of GaN/Air DBR and the four period GaN/Air-gap based DBR and they are the following:

Sample 1 - E-3689 - from top to bottom:

- The thickness of Si_3N_4 mask is 100nm
- The thickness of the first layer GaN is 195 nm
- The thickness of the sacrificial layer InGaN is 20 nm
- The thickness of c-plane GaN template is 10μm (doped)
- C-Sapphire substrate

Sample 2 - E-3690 - from top to bottom:

- The thicknesses of GaN layers are 50nm $\times 4periods$
- The thicknesses of the sacrificial layers InGaN are 25 nm $\times 4periods$
- The thickness of c-plane GaN template is 10 µm (doped)
- C-sapphire substrate.

For the fabrication of microscopic geometrical patterns (mesas) on the surface of the samples, the e-beam lithography method was used. The sample E-3689 was separated as a chessboard 3X3 and sixteen patterns were manufactured in each area (box) of 600 $\times$ 600 µm.

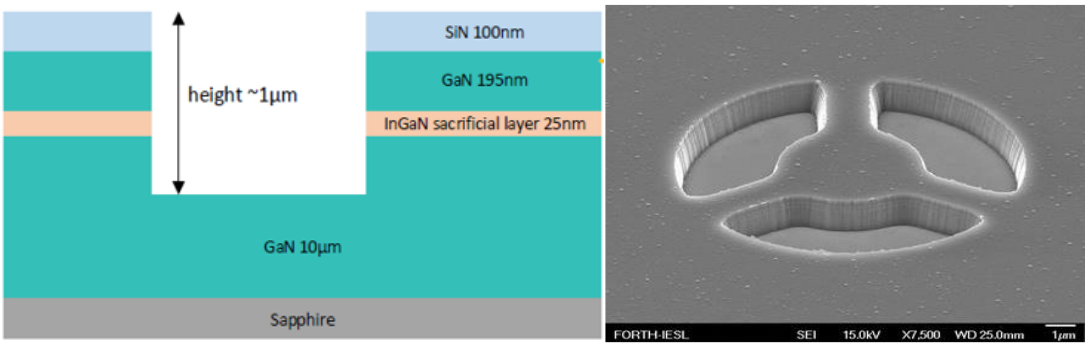

***Figure 3.3**: Schematic illustration of the sample and mesas presentation (E-3689).*

For the sample E-3690, an area 1x1 mm was used and sixty-four mesas were fabricated. The geometrical patterns present different diameters in order to observe the difference in the etching processing and in order to create the air-gap without the patterns collapsing.

In **Fig. 3.4,** the distance and the diameters of the mesas are presented.

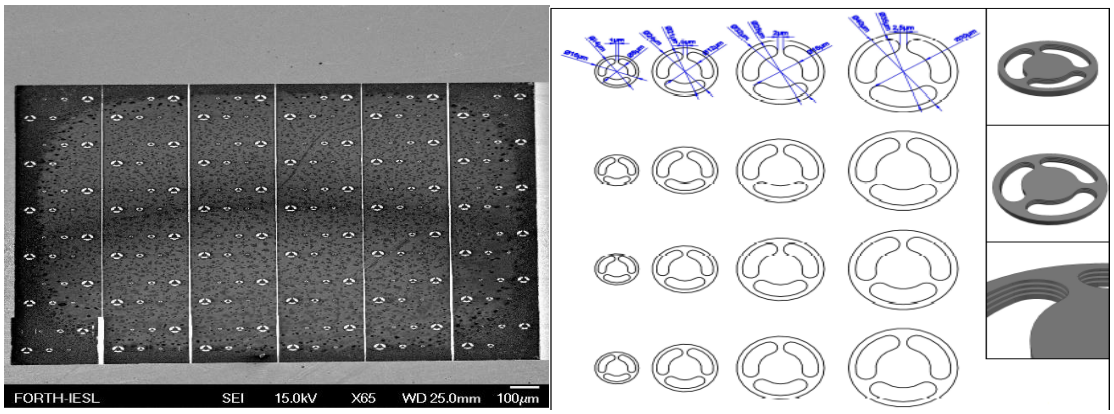

***Figure 3.4**: Geometrical patterns on 1x1mm area of E-3690 sample.*

The photo-electrochemical etching experiments were carried out in a photochemical cell, which is made from Teflon. The backside of the cell consists of a hole, which is covered with an intermediate cone ring with diameter about 1mm, on which the semiconductor is placed. Opposite the semiconductor, in the front side of the cell, there is a quartz window that allows the semiconductor to be excited with wavelengths in the ultraviolet range. Furthermore, on the top right side of the cell, a platinum wire (Pt) is suspended inside the cell. In addition, on the upper place of the cell a bigger hole exists that allows the access in it for inducing the electrolyte. Finally, at the bottom of the cell a smaller hole is designed that allows the draining of the solution after the experimental process is finished.

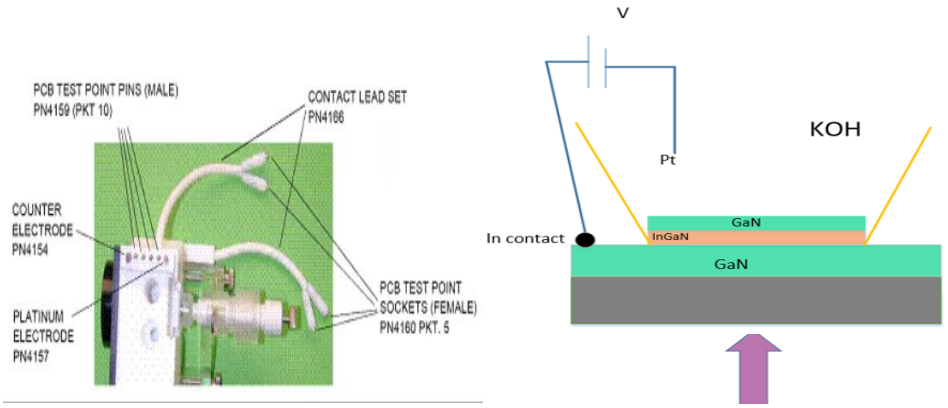

***Figure 3.5**: Schematic presentation of photochemical Teflon cell and the sample in contact with the electrolyte, to perform lateral etching.*

The experiments were performed at room temperature and an Indium (In) contact on the samples was applied, operating as the cathode, while the platinum wire in the cell operates as the anode. The excitation source is a diode laser 405 nm (energy greater than the band-gap of the sacrificial layer) and the electrolyte is KOH since, from other experimental processes, KOH solution yields

smoother etched surfaces and sharper sidewalls on the samples. The experimental process starts by applying reverse bias on the samples, as can be seen from the illustration in **fig 3.5**.

When applying the reverse bias, the GaN n-doped layer catalyzes the field application by intensifying the bending of the zone, as discussed in **section 3.2**, which operates similar to the Schottky zone with the aim of trapping the holes in the semiconductor-electrolyte interface, while the electrons are attracted to the interior of the semiconductor.

The above process can be described by the following chemical reactions:

$$2\ln GaN + 6h^{+} + 6OH^{-} \rightarrow (\ln, Ga)2O^{-3} + 3H_2O + N_2 \uparrow$$

$$(\ln, Ga)2O_3 + 6OH^{-} \rightarrow 2(\ln, Ga)O^{-3} + 3H_2O$$

In the first chemical reaction, the oxidation reaction is presented, which is induced by holes (h) in the valence band. The holes that are at the solution and the semiconductor interface have the ability to act as a broken chemical bond and thus, they have the ability to allow the ionic dissolution of the InGaN. The separated OH ions from the electrolyte react with the holes held to the surface of the sample to form by-products, which are in the form of H_2O and nitrogen (N_2). The second reaction refers also to by-products formed during the experiment.

3.3.1 Experimental PEC Procedure

SAMPLE E-3689: FIRST EXPERIMENTAL SERIES

A series of PEC experiments were performed for the fabrication of the mono-period GaN/Air-gap DBR. In the first experimental series, the contact of the photo-beam and the sample was made backside for the protection of the surface of the sample.

The power of the photon beam was formed at P = 12mW. This decision was made because the higher photonic stimulation strengthens the carriers that can actively participate in the process, contributing to the increase of the photocurrent and the reduction of the total time of the experiment. In addition, the electrolyte concentration was adjusted to C = 0.0004 M. The given voltage from the power supply remained constant at V = 4 Volt.

It is important to note that low voltages, i.e. 0.3-3.5 Volt, can result in a low drawing current and to a great increase of the time of the experiment. At the same time, the rather high voltages create excessive drainage, significantly reducing the experimental process but preventing the uniform exposure of the current to the surface of the semiconductor, receiving unevenness and roughness in the sidewalls of the DBRs. In the process, a periodic shutter was also used. The use of this shutter with a pulse period of 5 seconds clearly shows that without the presence of the photonic beam there is no production of photocurrent, thus the PEC process cannot occur.

In the next **Fig. 3.6**, a typical I-t diagram that was taken from the measurements is presented.

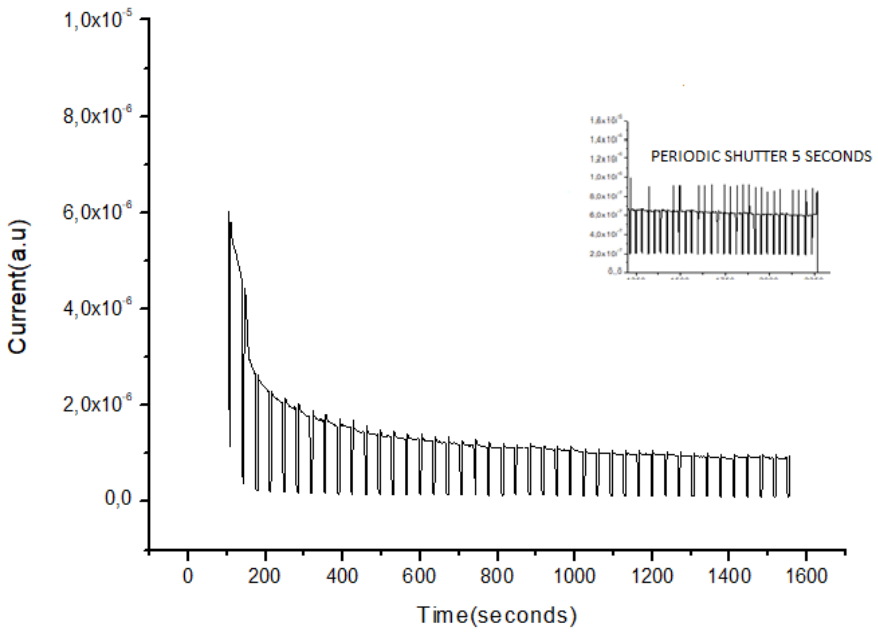

***Figure 3.6**: Typical I-t measurement of the PEC-selective process, presents the degradation of the photocurrent in relation to time.*

From the above **Fig. 3.6**, the proportional dependence of the photocurrent and the etch rate is observed. As the photo-electrochemical wet-selective etching progresses, the photocurrent induces. When the photocurrent is zero the etch process stops itself. In the following two figures a series of SEM images are presented for further understanding of the process.

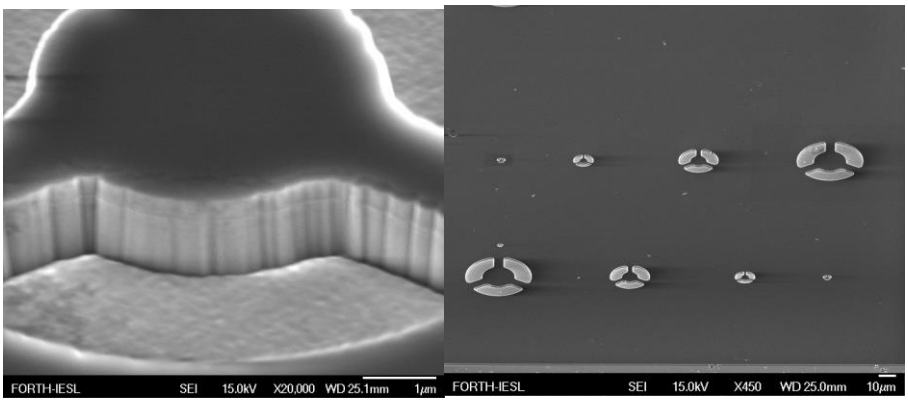

***Figure 3.7**: SEM images before etching sample E-3689.*

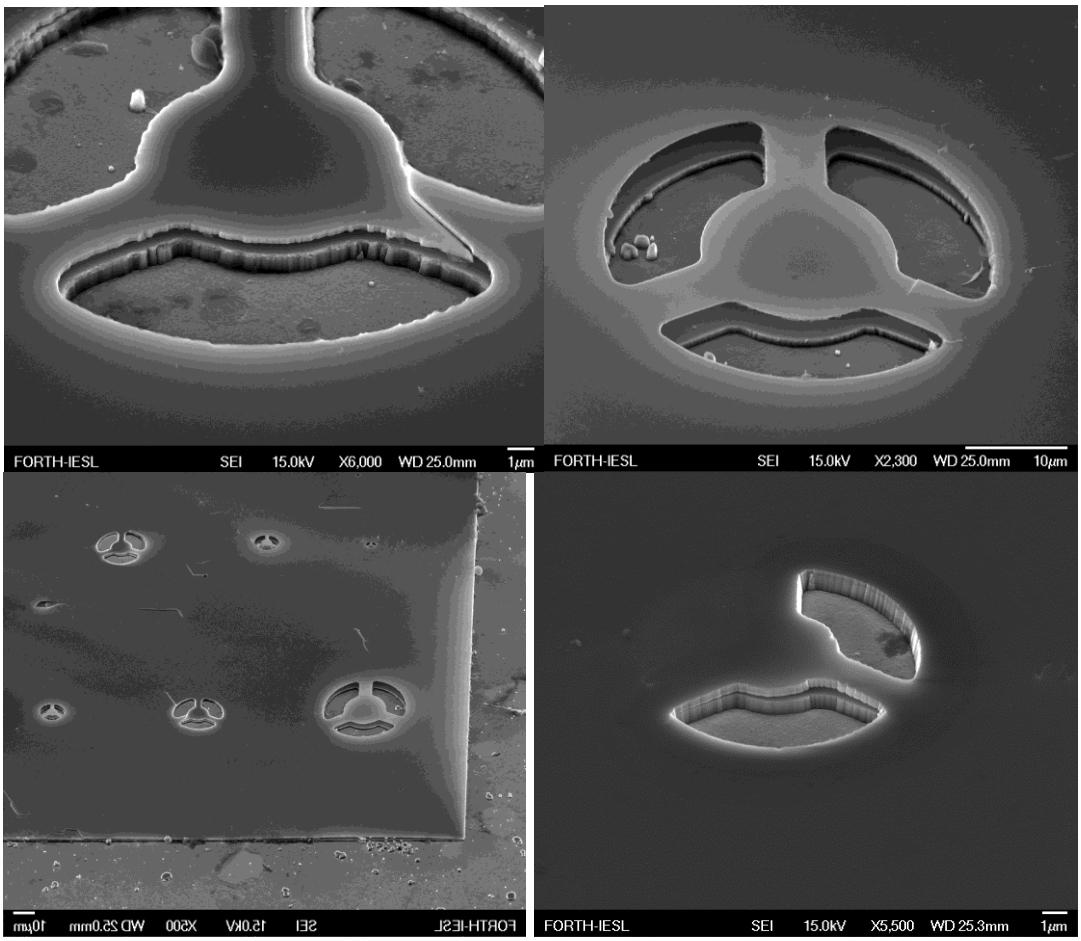

***Figure 3.8**: SEM image of GaN/air-gap one period, backside after PEC processing.*

From the SEM images above, it is clear that the etch process has been carried out, therefore the sacrificial InGaN layer has been removed. It is also observable that during and after the experiment, there is an absent of by-products. The by-products from the oxidation have been removed with a process that is called self – cleaning, and will be discussed in the next sections.

SAMPLE E-3689 - SECOND EXPERIMENTAL SERIES

In the second series of experimental procedures followed for this sample, the contact with the photo beam occurred from the front side of the surface of the sample, as observed in the following scheme in **Fig. 3.9**.

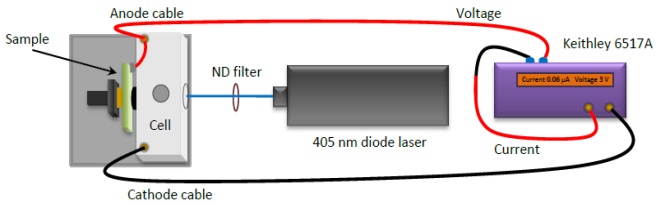

***Figure 3.9**: Schematic presentation of experimental setup-front side.*

This process was performed for better observation of the behavior of the by-products on the surface of the semiconductor, during and after the experiments, with the aim of a better understanding of the process of the self-cleaning.

In these series, the power of the photo-beam used, was set to P = 7 mWatt, while the bias and the concentration remained the same, V = 4Volt and C = 0.0004M respectively. It is important to note that the sample was coated with a silicon nitride mask of 100nm in thickness, as mentioned above, with intention to protecting the surface of the heterostructure.

As can one see from the **Fig. 3.10** of these experimental series, by reducing the power of the laser the duration of the experiment was increased for the removal of the sacrificial layer. Furthermore, no pulse periodic shutter was used.

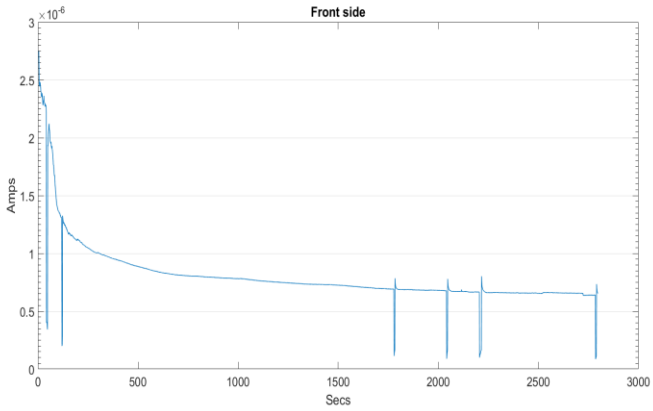

***Figure 3.10**: Typical I-t measurement, front-side.*

The sudden drop in the current is due to the instantaneous blocking of the laser beam in the photocurrent observation.

Under certain experimental etch conditions, the engraved surface of the semiconductor has the ability to self-clean. This can be translated from **Fig. 3.10** as the release of the photocurrent due to the accumulation and gradual disintegration of the oxide layer.

As can be seen by the next series of SEM images in **Fig. 3.11**, the oxides on the surface are not always dissolved.

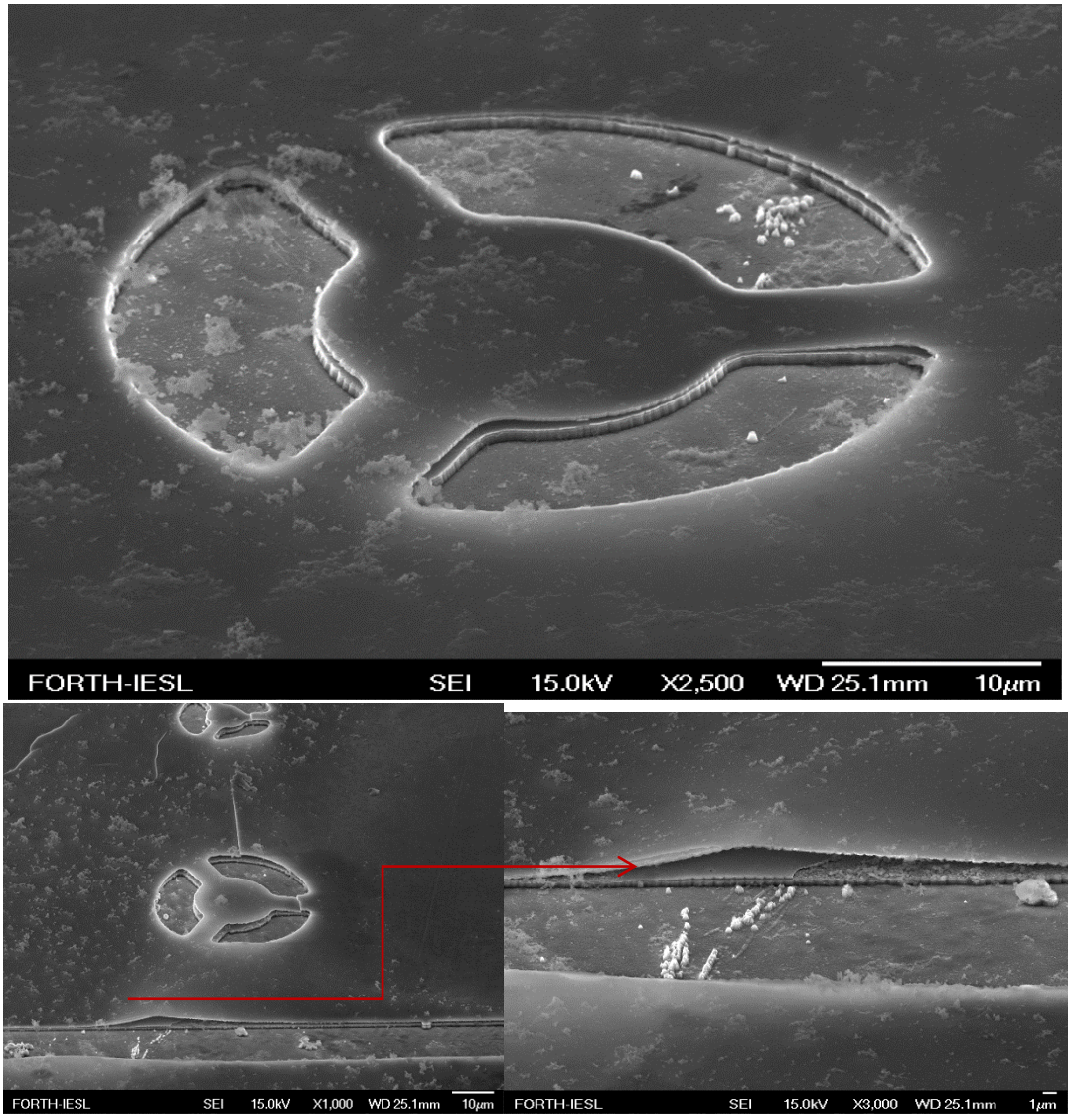

***Figure 3.11**: SEM images oxide by-products formation*

Conclusively, from the comparison of the SEM data in combination with the I-t diagrams, it is viable to express that the degradation of the photocurrent that is spotted is due to the oxides formation that take place when the laser beam has direct contact with the sample. The curve formed on the so-called “membrane” is due to the strain relaxation of the GaN layer.

For further data, the surface of the sample was removed with the help of carbon tape to observe optically the smoothness of the extracted membranes, as well as to see if any residues of the InGaN layer have remained.

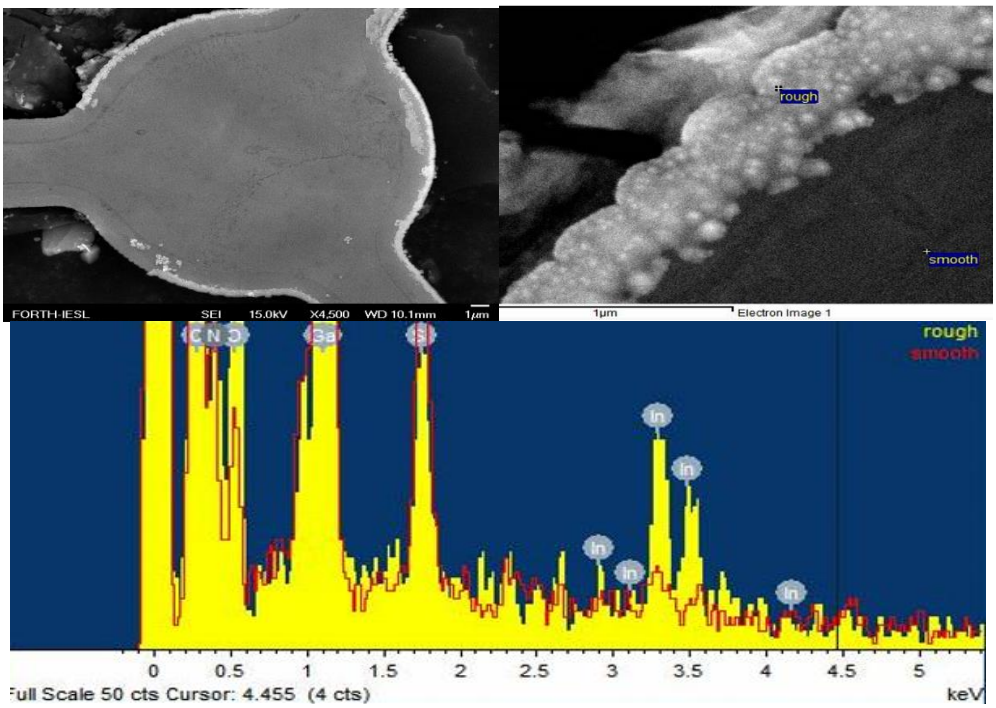

***Figure 3.12**: SEM image and components diagram the InGaN has not been removed.*

From the above schemes, it can be understood that if one manages to block periodically the excitation beam, i.e. with a pulse shutter, then the dissolution of the oxide layer takes place and can expose another interface of the sacrificial layer in the electrolyte. So, one can culminate that an experimental process with a Shutter gives time for self-cleaning and for further etching, as happened in the first series of the experimental procedure.

SAMPLE E-3690 - EXPERIMENTAL SERIES

The second sample submitted to the PEC wet selective etching process consist of fiver alternating periods of GaN. The goal at the end of the experiment is the creation of air-gap DBRs with four periods of air to achieve higher reflectivity, as discussed in **Chapter 2**.

With this heterostructure, many challenges had to be overcomed, due to its complexity. These challenges mostly concern the difference in the lattice constant. Lattice constant refers to a parameter of crystal structures that describes the adaptability between two or more different layers of materials during epitaxial growth. When the lattice constant between two layers differs, then strains are introduced into the materials and result to roughness or cracks on the surface of the layers during the epitaxial growth.

The structure of the sample E-3690 consists of alternating GaN and InGaN layers. However, this choice brought many challenges because there is a large lattice mismatch between these two layers. This leads to high strain on the surface of the structure, as shown in next **Fig. 3.13**, and

affects the performance of the experiment, as well as degrading the quality of the sample for future use.

Before the process, the photon beam came in contact with the structure from backside with power P = 10mWatt. Although, as observed for sample E-3689, this protects the surface of the samples, due to the abnormalities presented the electrolyte penetrates its macroscopic cracks, attacking its facets. As mentioned above, GaN and generally nitrides type-III exhibit a wide resistance to acid and alkali solutions. This can lead to lateral and also vertical etching of InGaN. The bias staid constant at V = 4Volts and the concentration of the solution decreased in value at $C = 3{,}2 \times 10^{-5} M$, following the linear relation between molarity of alkali solutions and pH, as presented in the next figure.

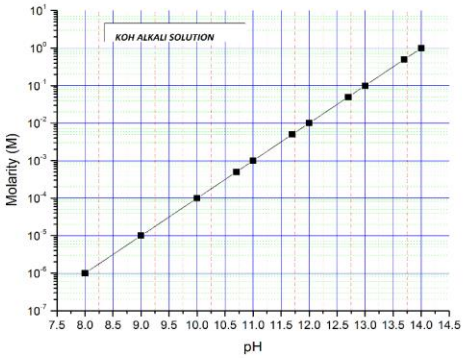

***Figure 3.13**: Linear relation between molarity and pH in alkali solutions.*

From **Fig. 3.14 (a)**, it is observed that the surface of the structure is damaged, it presents cracks and unevenness. Furthermore, fearing the possible collapse of the semiconductor's structure, the experimental time did not exceed twenty minutes. In **Fig. 3.14 (b)** the sample after the PEC etching process is presented.

(a)

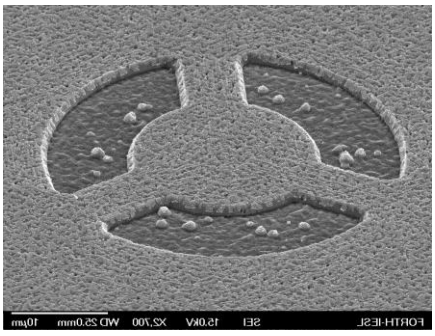

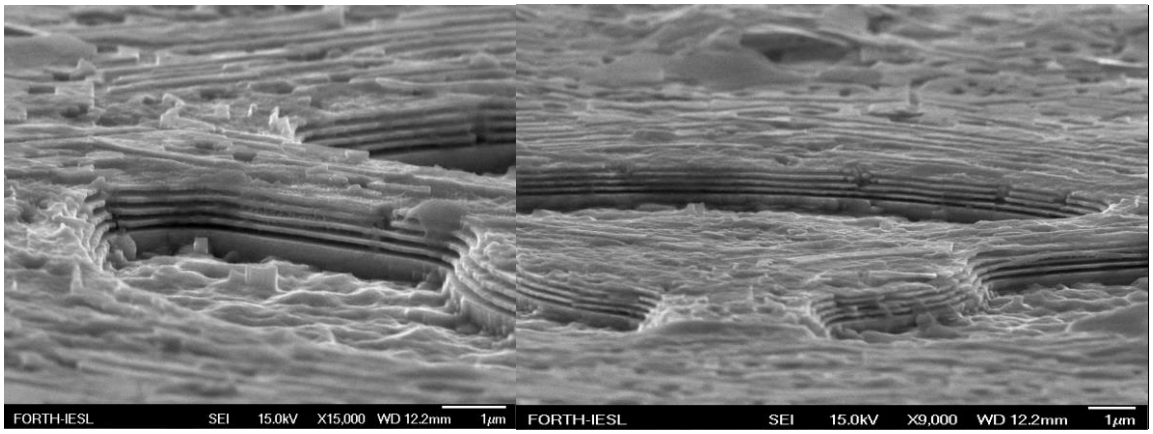

***Figure 3.14**: SEM image. Surface of the structure before (a) and (b) after PEC lateral etching.*

As shown in the figures above, no InGaN infusion is observed on the surface of this structure despite the difficulties it presented during the experiment. In addition, the sidewalls of GaN layers that were taken through the procedure are quite smooth and sharp.

The overall data obtained through these series of experiments are quite promising as they can lead to the fabrication of Air-gap GaN based DBRs with high reflectivity values such as the theoretical ones presented in ***Chapter 2,*** if the same experimental approach is performed with better quality samples.

3.4 Micro – PEC

Considering the state of the art of Photo-electrochemical etching, as well as the experimental data discussed above, an effort was made so that the process would take place at microscopic level. Taking advantage of the fundamental principles of modern optics, an experimental arrangement was set up which allows visual observation of the surface of the semiconductor magnified by ~ 100μm during the etching process.

The advantage offered by this experimental set up is that the PEC lateral etching procedure takes place individually for every geometrical pattern, with diameter from 20μm to 5μm on the semiconductor's surface, in order to avoid the total subsidence of the samples surface. The sample is illuminated with light that passes from two different mediums, the first of which is of aqueous solution and the second medium is air. After that, the image of the illuminated sample passes through objective lens and then, with the help of a mirror, it is redirected to determine the final magnification of the respective optical path and end through a lens of focal distance 200mm to the CCD cam.

As far as the excitation beam is concerned, it passes through an iris and two Nd filters with the purpose of reducing the power of the beam and then it goes through a beam splitter in order to be redirected into two directions. The first one is that it passes through the objective lens, which is at a specific focal distance. The laser pattern is focused on the semiconductor sample. The second direction that it follows is through the beam splitter and, with the help of the mirror, it is redirected to the camera.

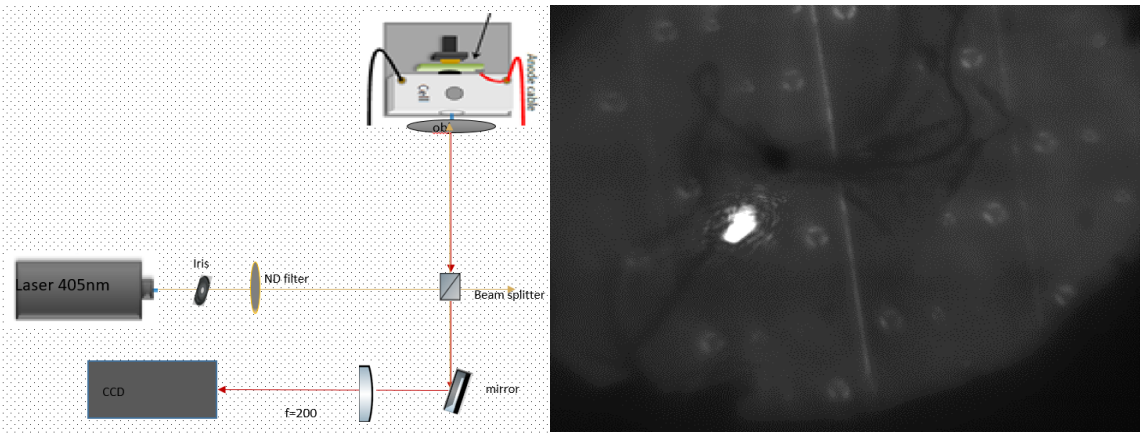

***Figure 3.15**: Micro PEC setup (a) and (b) imaging of the sample.*

The experimental parameters that were used are the following:

- $M_{KOH} = 4 \times 10^{-4}$ Molarity
- $V = 4\,Volt$
- The Power of the excitation beam was adapted at 0,1mW

In the above **Fig. 3.15**, the magnified surface of the sample and the excitation beam are presented.

The saturation observed by the excitation beam, illustrated during the imaging, can be controlled with the use of the iris and the Nd filters for understanding its exact diameter, which is about 40 μm, in relation to the largest geometrical pattern with diameter 20 μm.

3.5 References

1. E. Trichas, Strong Light-Matter Coupling in GaN Microcavities
2. P. A. Kohl, Photoelectrochemical Etching In Semiconductors, IBM Journal of Research and Development, 1998
3. R. Memming, Semiconductor Electrochemistry, Second Edition, ISBN 978-3-527-31281-8
4. J. Reichman, The currentvoltage characteristics of semiconductor electrolyte junction photovoltaic cells, Applied Physics Letter

5. S. Chandra, R. K. Pandey, Semiconductor Photoelectrochemical Solar Cells, Review Article phys. stat. sol. (a) 73, 415, 1982

6. C. Youtsey, I. Adesida, G. Bulman, Highly anisotropic photoenhanced wet etching of n - type GaN

7. X. Xiao, A. J. Fischer, M. E. Coltrin, P. Lu, D. D. Koleske, G. T. Wang, R. Polsky, J. Y. Tsao, Photoelectrochemical etching of epitaxial InGaN thin films: self-limited kinetics and nanostructuring, 20

CHAPTER 4. CONCLUSION AND DISCUSSION

To summarize, PEC procedure of III-V semiconductors' group has been extensively used through the decades to form unique structures in optoelectronic devices. In this thesis, the Photo-electrochemical wet lateral selective etching has been developed, with the aim of forming structures with a promising use as air-gap based DBRs.

Through XRD and photoluminescence measurements, the thicknesses of the samples E-3689 and E-3690 were validated to see if there were any exclusions from the theoretical approaches. In addition, from the theoretical models of these structures that were presented by period vs reflectivity and operational wavelength vs reflectivity diagrams, it is understood that the high contrast in the refractive index between GaN layer and air, provides a high reflectivity value at about 67% even for one alternating period of GaN/Air.

In the experimental procedures, an excitation beam and aqueous KOH solutions in extremely low concentrations were used. From the photocurrent versus time diagrams that were extracted, the direct relation between those two can be seen, along with the etch process. When the dignified photocurrent approaches the value of zero, the etch process stops itself.

Furthermore, from the SEM images that were taken from the samples, one can notice that the indirect photo-stimulation in relation to the surface of the hetero-structures (backside excitation) provides betters results, concerning the quality and the smoothness of the membrane's sidewalls and their surface. In addition, after the experiment the membranes were lifted with carbon tape in order to observe if any traces of the InGaN (sacrificial layer) have remained.

From those images, and by comparing them with old data, information about the self-cleaning process, that takes place during the experiments, were taken. It became known that if the excitation beam is blocked periodically (for example with a pulse shutter) during the etching process, then the dissolution of the oxide layer could clean the etched surface and expose another InGaN interface in the electrolyte. The above, can provide time for the self-cleaning and further etching, as happened with the old data.

Taking into account all the above, the etching process was conducted on the four alternating periods of GaN/InGaN sample. Due to the bad quality of its surface, the experimental parameters and the self-cleaning process were exploded to obtain the desirable air-gap without the disintegration of the GaN layers, as had happened before. The geometrical patterns that were fabricated on the surface of the semiconductor helped to obtain the desirable results, as was shown from SEM images and the photocurrent vs time diagram in **Chapter 3**. This is very promising considering that the theoretical reflectivity spectrum for these types of structures is offering 99% values in comparison with forty or sixty periods of alternating materials, due to the index contrast.

Moreover, by taking into consideration the preservation of the samples, a micro-photo-electrochemical etching set up was arranged for the optical observation of each mesa during the experimental procedure, simulating the parameter on a class surface of 30 μm. This arrangement presented many challenges, including the alignment of the excitation beam with the image of the sample. This idea of such an arrangement is very promising and can lead to new approaches, as far as the PEC process is concerned, for the fabrication of air-gap DBRs.

4.1 Towards the ideal microcavity

As discussed in **Chapter 2**, the structures that have the ability to confine both photons and electron-hole pairs are called micro-cavities. A microcavity consists of an effective medium that can be either organic, inorganic or hybrid, which is surrounded by metallic mirrors or DBRs structures. The QW are located in the maxima of the electric field for efficiency and both the active medium and the cavity are tuned in the same energy. The schematic representation of a planar micro-cavity with DBRs is presented in **Fig 4.1** below.

***Figure 4.1**: Schematic Illustration of a planar microcavity.*

The micro-cavity is formed when the thickness of the cavity is integral multiple of half of the operational wavelength $L_c = m\lambda_0/2$, where m, refers to an integer. The reflectivity spectrum of the microcavity differs in relation to that of a DBR, as it presents a characteristic dip at the operating wavelength.

Given that the air-gap DBRs present high reflectance spectrum, a theoretical microcavity with five periods of GaN/Air DBRs and active medium of InGaN quantum wells was fabricated.

The future perspective is the fabrication of a high Q factor microcavity featuring Air-Gap DBRs. **Fig 4.2** presents the reflectivity spectrum of such a micro-cavity tuned at λ=450 nm with refractive index of GaN at n=2.5.

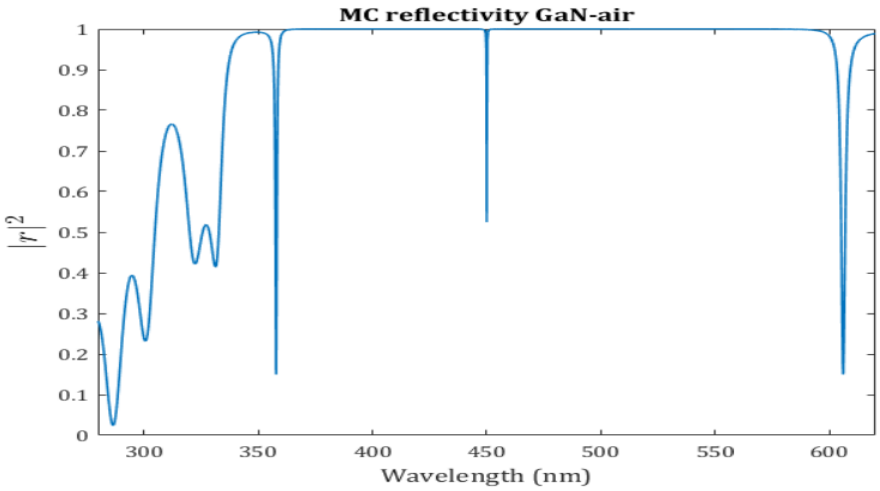

***Figure 4.2**: Reflectivity spectrum of ideal theoretical micro-cavity with air-gap DBRs*